# Times associated with source-to-sink propagation of environmental signals during landscape transience

**Stefanie Tofelde[1*], Anne Bernhardt[2*], Laure Guerit[3], Brian W. Romans[4]**

[1]Institute of Geoscience, University of Potsdam, Potsdam, Germany.

[2]Institute of Geological Sciences, Freie Universität Berlin, Berlin, Germany.

[3]University of Rennes, CNRS, Géosciences Rennes-UMR 6118, F-35000 Rennes, France.

[4]Department of Geosciences, Virginia Tech, 926 West Campus Dr., Blacksburg, VA 24060 USA.

*** Correspondence:**
Stefanie Tofelde, tofelde@uni-potsdam.de

Anne Bernhardt, anne.bernhardt@fu-berlin.de

**Keywords: signal propagation, landscape transience, source-to-sink, stratigraphy, response time**

**Abstract**

Sediment archives in the terrestrial and marine realm are regularly analyzed to infer changes in climate and tectonic boundary conditions of the past. However, contradictory observations have been made regarding whether short period events are faithfully preserved in stratigraphic archives; for instance, in marine sediments offshore large river systems. On the one hand, short period events are hypothesized to be non-detectable in the signature of terrestrially derived sediments due to buffering during sediment transport along large river system. On the other hand, several studies have detected signals of short period events in marine records offshore large river systems. We propose that this apparent discrepancy is related to the lack of a differentiation between different types of signals and the lack of distinction between river response times and times related to signal propagation. In this review, we (1) expand the definition of the term 'signal' and group signals in sub-categories related to hydraulic grain size characteristics, (2) clarify the different types of 'times' and suggest a precise and consistent terminology for future use, (3) compile and discuss factors influencing the times of signal transfer along sediment routing systems and how those times vary with hydraulic grain size characteristics, and (4) discuss the resulting consequence regarding signal preservation in stratigraphy. Unravelling different types of signals and distinctive time periods related to signal propagation addresses the discrepancies mentioned above and allows a more comprehensive exploration of event preservation in stratigraphy – a prerequisite for reliable environmental reconstructions from terrestrially derived sedimentary records.

# Table of Contents

## 1 Introduction

Sediment archives are regularly analyzed to reconstruct climatic and tectonic conditions of the past. Most terrestrial sediments are initially produced on hillslopes in mountain regions and are subsequently transported by fluvial systems to subsiding continental lowlands or to the coastal ocean, and further across the shelf and continental slope to deep marine basins (**Fig. 1**). The transport pathways of sediments from a zone of production (source) through a transfer zone to final deposition (sink) are generally described as sediment routing systems (SRSs) (Schumm, 1977; Castelltort and Van Den Driessche, 2003; Allen, 2008a, 2017). To reconstruct past conditions from deposited sediments, it is assumed that changes in climatic or tectonic boundary conditions generate so-called ‘environmental signals’ within the sediment. Environmental signals (signals hereafter) typically refer to measurable changes in the amount of produced, transported, and deposited sediments that can be related to changes in environmental boundary conditions (Romans et al. 2016 and references therein). Changes in environmental boundary conditions are temporary or sustained adjustments in tectonic uplift or subsidence rates, in climatic parameters, or in anthropogenic land use. However, experimental, numerical and field studies have shown that not all signals generated in the erosion zone are faithfully transmitted to the sink, but can be delayed, buffered, modified, or even destroyed during transport along SRSs (Jerolmack and Paola, 2010; Simpson and Castelltort, 2012; Armitage et al., 2013; Blöthe and Korup, 2013; Godard et al., 2013; Forzoni et al., 2014; Braun et al., 2015; Romans et al., 2016; Straub et al., 2020). It was suggested that signals in the form of sediment flux pulses are only faithfully transmitted to the sink if the period of changes in boundary conditions exceeds the response time of the river (Paola et al., 1992; Castelltort and Van Den Driessche, 2003; Li et al., 2018a). The river response time is the required time to achieve a new equilibrium river profile after a change in boundary conditions. Hence, for reliable reconstructions of past boundary conditions from sediment deposits it is essential to investigate the linkages between processes and times of signal transfer with processes and timescales of river adjustment.

Paola et al. (1992) suggested that river adjustments after a change in boundary conditions in alluvial rivers can be approximated as diffusive-like processes and the according response time, $T_{eq}$ [s], of a 1D fluvial profile can be estimated as:

$$T_{eq} = L^2/K \qquad \text{(eq. 1)},$$

where $L$ [m] is the length of the transfer system and $K$ [m$^2$ s$^{-1}$] its coefficient of diffusivity. Hence, response times greatly depend on the size of the river basin. Allen (2008b) considered landscapes with response times, $T_{eq}$, greater than the periodicity of changes in boundary conditions as ‘buffered’, while landscapes with response times shorter than the period of changes in boundary conditions as ‘reactive’. Following this approach, faithful signal transmission should be limited to reactive landscapes, such that short period climate cycles should not be transmitted through large rivers systems (Paola et al., 1992; Castelltort and Van Den Driessche, 2003; Allen, 2008b; Li et al., 2018a; Straub et al., 2020).

A lack of signal transmission of short period climate cycles in large river systems was presented by Métivier and Gaudemer (1999). Following equation 1, the authors obtained river response times on the order of $10^5$ to $10^6$ yr for some of Asia’s largest rivers. They found no major differences between the present-day sediment discharge for some of Asia’s largest rivers and the Quaternary-averaged sediment discharge reconstructed from mass accumulation in the corresponding sedimentary basins. Hence, sediment discharge at the river’s outlet was constant, despite known climate oscillations throughout the Quaternary on the order of $10^4$ yr (e.g. 20 and 40 kyr Milankovitch cycles). Métivier and Gaudemer (1999) interpreted those river systems as buffered.

However, other studies indicate that several large river systems show signal propagation occurring at an order-of-magnitude shorter timescale than their according response times. For example, Castelltort and Van den Driessche (2003) calculated the river response times of 93 of the largest rivers worldwide using equation 1. The calculated response time of the Mississippi River is between 124 - 248 kyr (Castelltort and Van Den Driessche, 2003). Yet, multi-modal mixtures of detrital zircons within the Mississippi submarine fan are changing over 10 kyr (**Fig. 1**; Mason et al., 2017; Fildani et al., 2018). Those provenance changes were interpreted by these authors to represent signals originating in the catchment, which were efficiently transferred to and preserved in the Mississippi delta and deep-sea fan. Therefore, signal transfer through the Mississippi SRS was rapid and an order-of-magnitude shorter than the theoretical response times (Mason et al., 2017; Fildani et al., 2018). Similarly, the Ganges River features a $T_{eq}$ of ~99 kyr (Castelltort and Van Den Driessche, 2003). However, system-wide changes in sediment flux and aggradation and incision cycles as contemporaneous responses to multi-millennial climate changes were observed in fluvial and deltaic archives along the Ganges SRS at time scales well below 99 kyr (**Fig. 1**, Goodbred, 2003). Within smaller SRSs along the western active margin of the Americas, offshore turbidite systems record late Pleistocene to Holocene climatic changes even with theoretical river response times of ~100 kyr (**Fig. 1**, Covault et al., 2010; Bernhardt et al., 2017).

In summary, short period climate changes seem to be recorded in marine stratigraphy offshore small and large river systems, although the according river response times of large river systems exceed the period of the climate changes. We propose, however, that this discrepancy is only apparent, as different concepts are compared. While each approach has its legitimacy, we believe that inconsistencies are caused by two issues:

(1) The lack of a differentiation between different types of ‘signals’ and according differences in signal propagation.

(2) The river response time is different from the time it takes for a measurable change in a sedimentary parameter to arrive in the sink.

Terrestrial and marine sedimentary archives are the result of a broad range of geomorphic processes along SRSs. Reliable environmental reconstructions from those archives therefore require interdisciplinary knowledge exchange, which relies on a common and precise terminology. To overcome any current deficiencies, we will (1) expand the definition of the term ‘signal’ and group signals in sub-categories related to hydraulic grain size characteristics (section 2), (2) clarify the different types of ‘times’ and suggest a precise and consistent terminology for future use (section 3), (3) compile and discuss factors influencing the times of signal transfer along SRSs and how those times vary with hydraulic grain size characteristics (section 4), and (4) discuss the resulting consequence regarding signal preservation in stratigraphy (section 5).

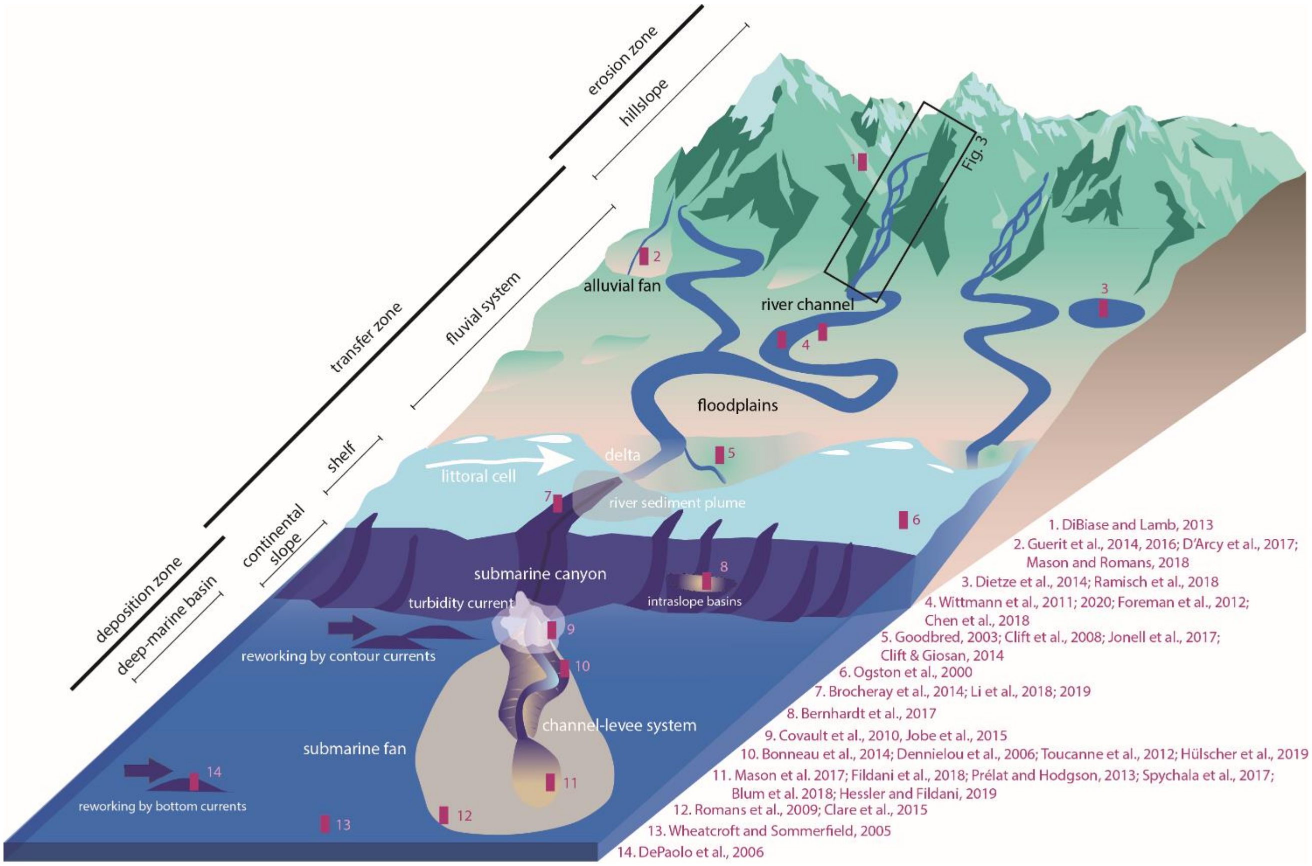


***Figure 1*** *Schematic sketch of a continental-scale sediment routing system (SRS) from the upland source to the deep-marine sink. SRSs are typically subdivided in a zone of erosion, sediment transfer and sediment deposition. On a continental scale, SRSs comprise five landscape segments including hillslopes, fluvial system, shelf, continental slope and deep marine basins. Sampling sites of sediment archives discussed in the text are indicated with magenta colored symbols. Black frame marks the erosion zone as discussed in Fig. 3.*

## 2 Definition of signal and hydraulic grain size fractions

Environmental signals are typically defined as changes in the amount of produced, transported and deposited sediment ($Q_s$ [$m^3$ $s^{-1}$ or kg $s^{-1}$]) in response to a change in boundary conditions (Romans et al., 2016 and references therein). Therefore, many analog-material and numerical modelling studies investigating the effects of changing boundary conditions on signal propagation focus on changes in $Q_s$ (e.g., Allen and Densmore, 2000; van den Berg van Saparoea and Postma, 2008; Simpson and Castelltort, 2012; Armitage et al., 2013; Coulthard and Van De Wiel, 2013; Li et al., 2018a; Moussirou and Bonnet, 2018; Tofelde et al., 2019). However, changes in boundary conditions do not only affect the amount of transported sediment, but can also alter the sediment grain size distribution (Armitage et al., 2011; Parsons et al., 2012; D'Arcy et al., 2016, 2017; Bataille et al., 2019) or its geochemical composition and detrital geochronological signature (Sharman et al., 2019; Lenard et al., 2020). Therefore, we expand the definition of an environmental signal: **We define an environmental signal as a measurable change in any sedimentary parameter of interest through time that can be linked to an environmental change.** The change in the parameter can either be temporary or sustained.

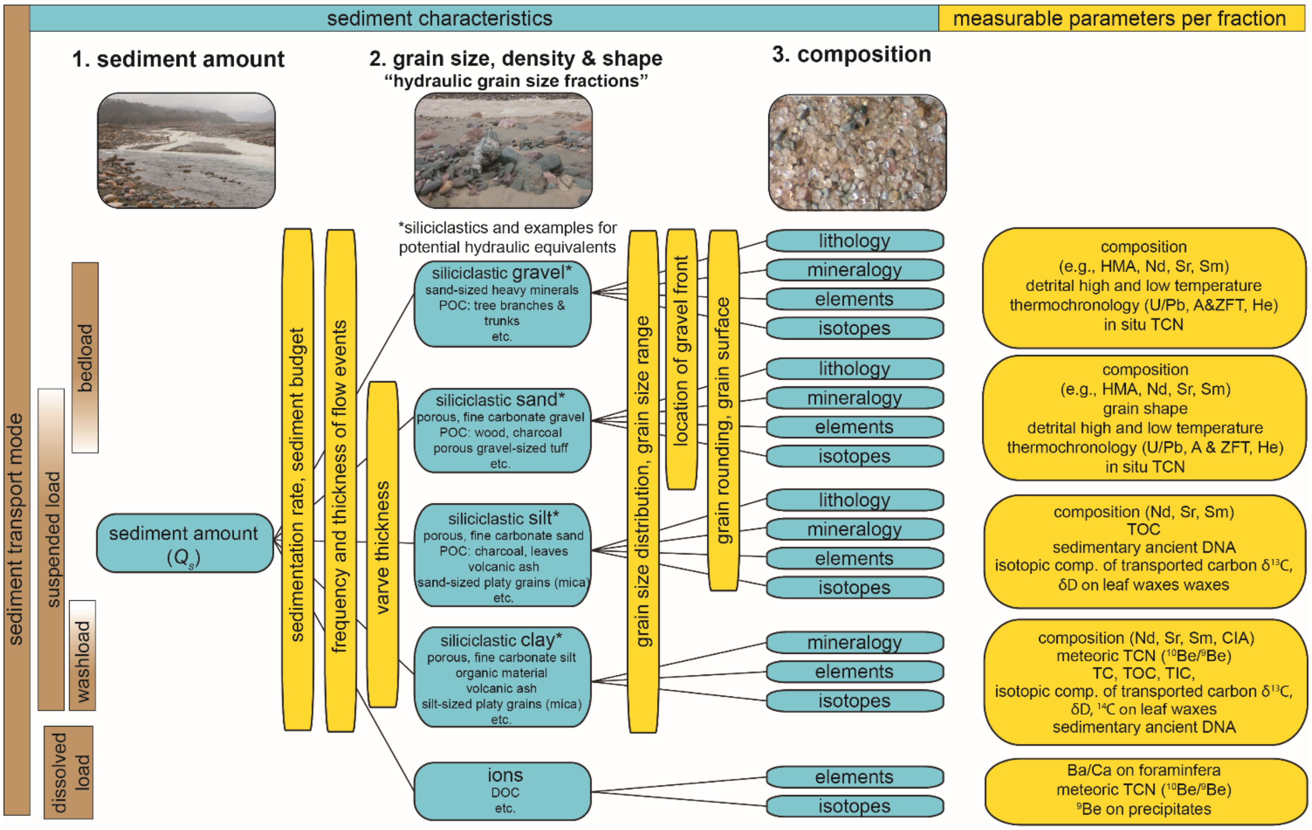


***Figure 2*** *Subdivision of signals based on sediment characteristics. Information on boundary conditions can either be stored in the amount of sediment transported per time, the grain size and shape distribution of that sediment and its changes through time, or within the changing sediment composition (blue boxes). Examples of parameters measured for environmental reconstructions (yellow boxes) can relate to any of those sediment characteristics. Several of those parameters, however, are only measured on a certain sub-fraction of the sediment. Sub-fractions can differ in their primary transport mode (brown boxes) and, hence, in times required to transport the sediment to the sink. Therefore, we suggest to subdivide signals based on hydraulic grain size fraction. A hydraulic grain size fraction is defined by the siliciclastic grain size, but includes other grains that are transported jointly due to similar hydraulic behavior. Please note that explicit classifications of certain materials to a specific hydraulic grain size fraction will be somewhat dependent on the study objectives and overall context and, thus, may differ from case to case. Also, the presented list of regularly measured sedimentary parameters (yellow boxes) is not exhaustive. TC = total carbon, TOC = total organic carbon, TIC = total inorganic carbon, POC = particulate organic carbon, DOC = dissolved organic carbon, TCN = terrestrial cosmogenic nuclides, HMA = heavy mineral analysis, A&ZFT = apatite and zircon fission track, CIA = chemical index of alteration.*

This definition is in accordance with the broad range of sedimentary parameters that are regularly measured in terrestrial and marine sediment archives (yellow boxes in **Fig. 2**). To summarize some commonly measured sedimentary parameters, we group them based on the sediment characteristics they are related to. We sub-divide sediment characteristics in (1) sediment amount ($Q_s$), (2) size distribution, density and shape of grains within a sediment package, and (3) sediment composition (blue boxes in **Fig. 2**). Parameters investigating the change in $Q_s$ through time include, for example, accumulation rates in one to three spatial dimensions (Covault and Graham, 2010; Guillocheau et al., 2012; Hinderer, 2012; Jobe et al., 2015; Guerit et al., 2016; Hülscher et al., 2019; Baby et al., 2020), the frequency and thickness of flow events (Mulder et al., 2001; Ducassou et al., 2008; Romans et al., 2009; Bernhardt et al., 2017) or varve thickness, particularly in lake sediment (Zolitschka et al., 2015) (**Fig. 2**).

The second group of parameters focuses on differences in the characteristics of grains within a certain sediment package, such as grain size distributions (Duller et al., 2010, 2019; Whittaker et al., 2010, 2011; Foreman et al., 2012; Parsons et al., 2012; Foreman, 2014; D'Arcy et al., 2017), median or other characteristic grain sizes ($D_{50}$, $D_{84}$, sortable silt; McCave and Hall, 2006; Schlunegger and Norton, 2015; Chen et al., 2018; McCave and Andrews, 2019; Watkins et al., 2020), the location of the gravel-sand transition in alluvial fans and river systems (Allen et al., 2015; Dubille and Lavé, 2015; Blom et al., 2017; Dingle et al., 2017, 2020; Armitage et al., 2018a), sorting and related textural characteristics (e.g., in glacio-marine sediments: Anderson et al., 1980; D'Orsay and Van De Poll, 1985; Pudsey, 1992; Helland et al., 1997; Passchier et al., 2019), or grain shape (Stanley and De Deckker, 2002; Kalińska and Nartišs, 2014).

The third group of parameters focuses on the sediment composition. Here, we consider sediment composition broadly (lithological, mineralogical, elemental and isotopic composition) and include the geochronological and thermochronological signature of detrital minerals. While some compositional parameters can be measured on an entire sediment (bulk) package, many are bound to a distinct grain size fraction only (**Fig. 2**). For example, magnetic susceptibility (Stoner et al., 1995; Da Silva et al., 2013) or XRF scanning (Weltje and Tjallingii, 2008; Kujau et al., 2010; Ramisch et al., 2018) of sediment cores measures the fraction of magnetic minerals and the elemental composition of bulk sediment, respectively. In contrast, high and low temperature detrital geo-/thermochronology is commonly analyzed on sand-sized heavy minerals, such as zircon or apatite (Weislogel et al., 2006; Heberer et al., 2011; O'Sullivan et al., 2018; Sharman et al., 2018). Paleo-denudation rates inferred from in-situ cosmogenic nuclides in detrital sediments are mostly measured in sand- and silt-sized quartz grains (Schaller et al., 2004; Val et al., 2016; Lenard et al., 2020), although comparisons of the same cosmogenic nuclide in different grain size fractions at the same location have revealed great variability between grain size fractions (Puchol et al., 2014; Carretier et al., 2015, 2019; Schildgen et al., 2016; Tofelde et al., 2018; van Dongen et al., 2019). Finally, fluvially transported organic compounds, for example leaf waxes from terrestrial plants, are regularly analyzed for their hydrogen ($\delta D$) and carbon ($\delta^{13}C$) isotope composition (Galy and Eglinton, 2011; Garcin et al., 2012; Sachse et al., 2012; Schefuß et al., 2016; Diefendorf and Freimuth, 2017). Oftentimes, the organic fraction is extracted from a certain sedimentary sub-fraction only, like the suspended load (e.g., Ponton et al., 2014), bedload (e.g., Galy et al., 2008; Galy and Eglinton, 2011) or from flood deposits (Hoffmann, 2015). To investigate past biodiversity, recent efforts advanced the analyses of ancient DNA preserved in sediments (Dommain et al., 2019), which may be transported together with siliciclastic silt and clay. For a detailed discussion on sediment generation and composition we refer to the recent review by Caracciolo (2020).

In summary, sedimentary parameters, and hence signals, are measured on different sediment fractions. Consequently, when investigating signal transfer and modification, we suggest to group sediments in '*hydraulic grain size fractions*' that are transported jointly (**Fig. 2**). **We define a *hydraulic grain size fraction* as a size range of siliciclastic sediments (e.g., sand, silt, etc.) and their hydraulic equivalents** (blue boxes in middle column, **Fig. 2**). For example, a sand-sized platy mica grain might be transported in the silt-sized hydraulic grain size fraction due to lower settling velocity compared to siliciclastics (Dietrich, 1982). Sand-sized heavy minerals, such as zircons and apatite, may be transported along with the *hydraulic grain size fraction* of small gravel due to the high density of zircons and apatites (4.65 and 3.2 g $cm^{-3}$, respectively) compared to quartz (2.65 g $cm^{-3}$). Similarly, particulate organic matter may be transported within the clay-sized *hydraulic grain size fraction* (Galy et al., 2008; Galy and Eglinton, 2011; Ponton et al., 2014). The dominant sediment transport mode (bedload, suspended load, wash load, dissolved load) varies with *hydraulic grain size fraction* (brown bars, **Fig. 2**). We acknowledge that the assumption of all grains within a *hydraulic grain size fraction* being transported jointly is a simplification. Grains with similar characteristics can, for example, be transported as suspended load or bedload (details in section 4). However, we base our sub-division on grain size and not on sediment transport mode, as ancient sediments can be assigned a *hydraulic grain size fraction* but not a transport mode, and because many parameters are measured on a certain grain size fraction.

The dominant transport mode of a distinct *hydraulic grain size fraction* exerts a major control on sediment transport times along SRSs. And sediment transport times, in turn, have direct implications for signal propagation and modification within SRSs (Chabaux et al., 2012; Carretier et al., 2019, 2020; Watkins et al., 2020). Therefore, we propose to investigate signal propagation not for bulk sediments, but for *hydraulic grain size fractions* individually. In order to do so, we discuss the impact of several boundary parameters on sediment transport times and whether or not the impact of those parameters varies with *hydraulic grain size fraction* (section 4). But first, in order to overcome any discrepancies related to inconsistent terminology, we distinguish relevant times of landscape response and times related to signal propagation (section 3).

# 3 Times related to landscape response and signal propagation

Landscapes respond to changes in boundary conditions by adjusting their topography. These adjustments are most pronounced in mountainous areas - the erosion zone (**Fig. 1**) - and can trigger severe changes in surface erosion processes and within the hydrological regime. Also, during landscape adjustment, sediments (and signals) are generated and transported along SRSs to an area of final deposition. Naturally, different times are of interest when studying landscape adjustment and landscape shaping processes, compared to studies that aim to reconstruct past environmental conditions from signals preserved in sediment archives. From a landscape evolution perspective, the recovery time of a landscape after a change in boundary conditions is of major interest, while from a reconstruction perspective, the primary interest is the timescale of signal generation and signal transport to the sink (or the time lag between a change in boundary conditions and signal arrival in the archive). In this section, we first discuss timescales of landscape response with a focus on river profiles, and second timescales related to signal propagation. The definitions of all timescales are summarized in figure 4 and the glossary.

## 3.1 Landscape response time

A landscape can either be in steady state (synonym: equilibrium) or in transient state, depending on whether the landscape is adjusted to the prevailing boundary conditions or not (e.g., Mackin, 1948; Howard, 1982; Allen, 2008). The adjustment of river profiles exerts a major control on the state of a landscape and, hence, the evolution of longitudinal river profiles following a change in boundary conditions is often studied in analog-material experiments (van den Berg van Saparoea and Postma, 2008; Rohais et al., 2012; Grimaud et al., 2016; Baynes et al., 2018; Tofelde et al., 2019; Savi et al., 2020), by using numerical models (Davy and Lague, 2009; Armitage et al., 2011, 2013, 2018b; Simpson and Castelltort, 2012; Goren et al., 2014; Braun et al., 2015; Nie et al., 2018), and sometimes in the field (Whittaker et al., 2008). **Figure 3** summarizes schematically the general response of a river following a step increase in water discharge ($Q_w$ [m$^3$ s$^{-1}$]) **(Fig. 3a1)** or tectonic uplift (as a relative base level drop or, in other words, a lowering of the limiting level below which the river cannot erode) (**Fig. 3a2**). The evolution is shown for four distinct moments in time, *t* [s], before ($t_0$) and after ($t_1$ *to* $t_3$) the change in boundary conditions. An increase in upstream $Q_w$ causes river incision along the entire profile (**Fig. 3b1**). Incision is most pronounced at the upstream end, resulting in a net reduction in channel gradient. In contrast, a drop in downstream base level triggers an upstream migrating knickzone (**Fig. 3b2**). A knickzone describes a reach along a river profile that is steeper than according upstream and downstream reaches.

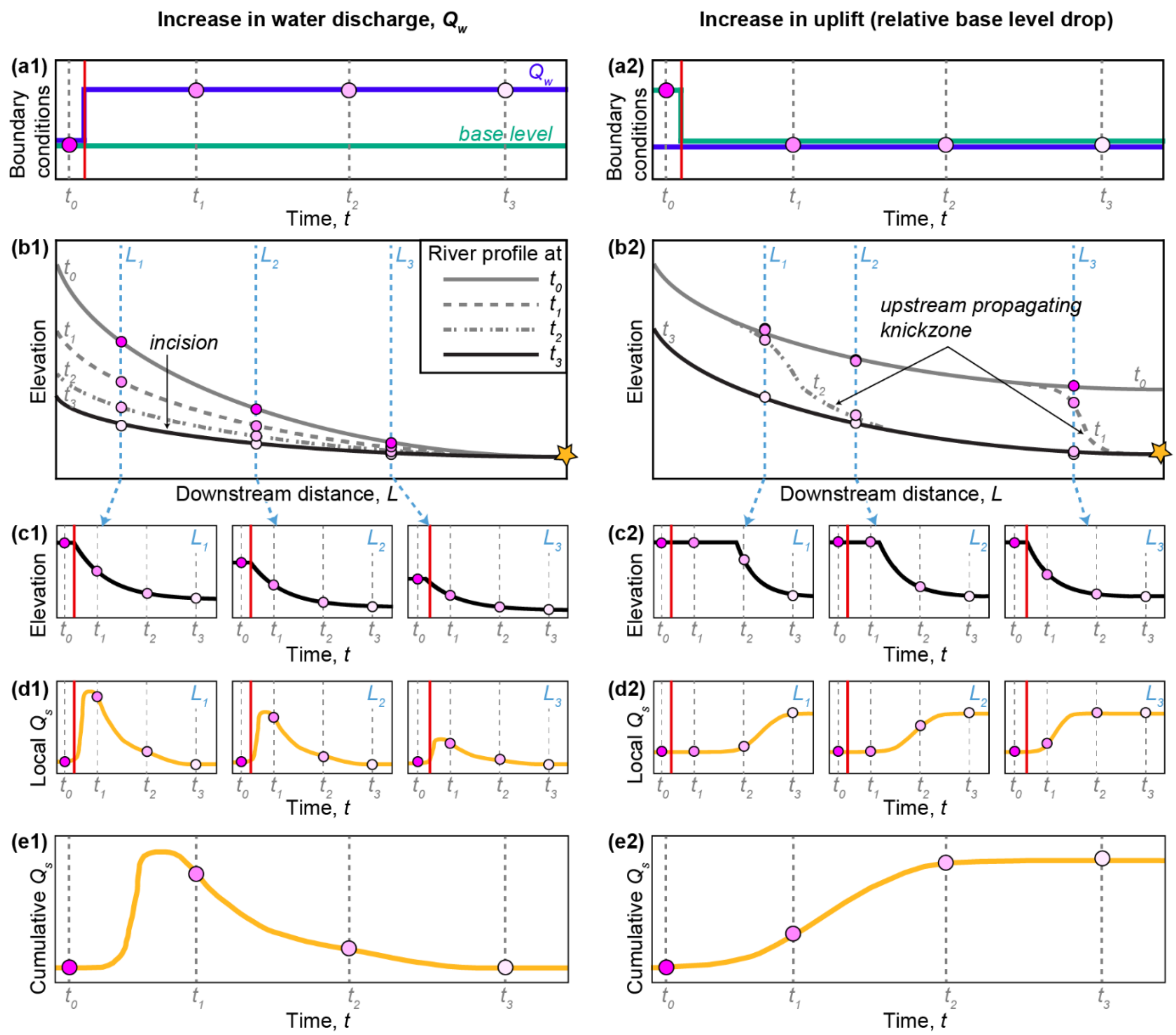


*Figure 3* *Response of the fluvial system to an increase in upstream water discharge (left panel) or a drop in downstream base level (right panel). (a) A step change in either water discharge (a1) or base level elevation (a2) occurs between the two points in time $t_0$ and $t_1$. (b) In response, the longitudinal river profiles adjust by rather simultaneous incision along the entire profile (b1) or by an upstream migrating knickwave (b2). (c) The change in elevation through time is displayed in detail for three locations along each profile $L_1$ to $L_3$. In addition to the topographic response of the landscape (b and c), signals - exemplary in the form of changes in transported sediment ($Q_s$) - are generated. Generated signals are displayed for each location ($L_1$ - $L_3$) within the landscape (d), and as an integrated signal measured at the catchment outlet (e). An increase in upstream $Q_w$ results in a temporary increase in $Q_s$ (d1 and e1). The amplitude of the generated signal differs along the river (d1). In contrast, a base level drop results in a sustained increase in $Q_s$ (d2 and e2). The increase in $Q_s$ differs in time between the three locations, as the knickzone needs to travel upstream, which requires time (d2).*

Topographic steady state is defined by no net changes in elevation, $z$ [m], through time, $t$ (Hack, 1960; Montgomery, 2001; Willett and Brandon, 2002). Following this concept, the *response time* of a landscape describes the period of landscape adjustment (landscape transience) after a change in boundary condition (e.g., Howard, 1982; Whipple, 2001; Allen, 2008; Straub et al., 2020). Depending on how response times are calculated (discussed below), it either describe the time to reach full steady state conditions (e.g., $dz/dt = 0$) or the time until the parameter of interest (i.e. $z$) has reached a fraction of its initial value. Sometimes, instead of *response time*, the term *adjustment time* (Schmid et al., 2018) is used. However, as different parts of the landscape respond to the same change in boundary conditions at different timescales (e.g., Hurst et al., 2012; Tejedor et al., 2017; Turowski, 2020), Allen (2008b) advised not to discuss response times too generally. Consequently, there have been a range of approaches of how to calculate response times for different parts within a landscape.

For signal propagation along SRSs, the response time of the river profile (*river response time*) is of particular importance. Following Allen (1974), Bull (1991) subdivided the river response in two components - the *reaction time*, which is the time lag between the onset of change in boundary conditions and the first topographic adjustment, and the *relaxation time*, which is the time period between the first topographic adjustment and the achievement of new steady state. Moreover, rivers are subdivided in detachment-limited and transport-limited endmembers. In detachment-limited rivers, river erosion is limited by the capacity of the channels to incise into their bed. In contrast, in transport-limited rivers erosion is limited by the capacity of channels to transport their sediment load. Following this, in numerical landscape evolution models the change in river elevation through space and time is most often described either by the advective stream power equation for detachment-limited rivers (Howard, 1994; Whipple and Tucker, 1999) or by a diffusion equation for transport-limited rivers (Paola et al., 1992; Wickert and Schildgen, 2019). The choice of equation to model the evolution of river elevation determines how river response times are calculated. Based on the stream-power law related equation for detachment limited rivers, Whipple and Tucker (1999) and Whipple (2001) derived equations for calculating the river response time based on the time required for the knickpoint to travel through the landscape length (equivalent to Bull's (1991) *relaxation time*; **Fig. 3b2**). The same approach can be used when channels are described as a continuum between transport- and detachment-limited behaviors (Davy and Lague, 2009; Carretier et al., 2016; Yuan et al., 2019a). For transport-limited rivers, the river response time for a 1D fluvial system was suggested to scale with channel length and the diffusion coefficient and can be calculated following **equation 1** (Howard, 1982; Paola et al., 1992; Allen et al., 2013). Paola (1992) termed this the *intrinsic equilibrium time.* It is important to note that the response time of a diffusion equation presumes a point change, for example a base level fall, and a subsequent dispersion of this change through the system. Alternatively, Howard (1982) and Simpson and Castelltort (2012) suggested that the time to reach the new steady state elevation profile in transport-limited channels can be estimated on the basis of mass balance for the volume of sediment that needs to be deposited or removed along the channel. Densmore et al. (2007b) and Allen (2008b) named all those theory-based (diffusion or advection) *river response times*, which describe the time of the river longitudinal profile to attain new steady state, *analytical response times*.

However, a response time can also be calculated when looking at the evolution of a certain landscape parameter only through time, that is for a single point in space or an average value of a certain area (e.g., local or catchment mean elevation, channel width, sediment discharge). A single parameter normally approaches new steady conditions after change in boundary conditions asymptotically, which can be approximated by an exponential equation (e.g., Kooi and Beaumont, 1996; Davy and Crave, 2000; Lague et al., 2003; Wickert and Schildgen, 2019). For example, while the evolution of the entire river profile through time (**Fig. 3b**) was described either by a wave or diffusion equation, the change in elevation at a single point along this river ($L_1$ - $L_3$ in **Fig. 3c**) through time behaves exponentially. From an exponential curve, *e-folding response times* can be calculated (Howard, 1982; Allen and Densmore, 2000; Densmore et al., 2007a; Allen, 2008b; Wickert and Schildgen, 2019). For an exponential decay curve as in **Figure 3c**, one *e-folding time* is equivalent to the time when the parameter of interest has decreased to 37% (≈1/e) of its initial value, or when 63% of the initial value is lost. After three *e-folding times*, 5% of the initial value remains (95% are lost). In case of exponential growth, one *e-folding time* is equivalent to the time when the parameter of interest has increased by a factor of *e* (~2.718). Hence, landscape evolution studies have also calculated response times by fitting an exponential curve to a measured time series of a certain landscape parameter, for example sediment discharge at the basin outlet (Densmore et al., 2007a; Armitage et al., 2013; Wickert and Schildgen, 2019), mean catchment erosion rate and mean fan deposition rate (Allen and Densmore, 2000), or provenance changes in discharged sediment (Sharman et al., 2019). Densmore et al. (2007b) and Allen et al. (2008b) named the response times measured by fitting an exponential curve to a parameter time-series the *relaxation time* (note that this relaxation time is different from the relaxation time defined by Bull (1991) and Allen (1974) as described above). However, it should be emphasized that an exponential curve asymptotically approaches a new steady state, but never reaches steady state. When an exponential curve is fitted to a parameter time series, stable conditions are assumed when the variability in parameter through time cannot be distinguished from background noise anymore (Kelly et al., 2011; Toonen et al., 2017). Hence, the *e-folding time* varies with the magnitude of noise in the parameter of interest. The magnitude of noise, in turn, may be related to the method of measurement instead of, or in addition to landscape-inherent properties, which complicates the comparison of response times between different landscapes. As *analytical response times* and *e-folding times* differ in a fundamental assumption – the first assuming the achievement of steady state and the latter not- the two concepts are incompatible.

### 3.2 Signal related times

In addition to landscape or river response times, specific signal-related times can be defined. Exemplary, we will discuss $Q_s$ signals generated by a step increase in $Q_w$ or a base level drop (**Fig. 3**). However, for the purpose of discussing signal related times in general, we then present a precise and consistent terminology applicable to all types of signals as defined above (**Fig. 4).**

Landscape adjustment after change in boundary conditions triggers signal generation. For example, a step increase in upstream $Q_w$ causes a temporary peak in $Q_s$ due to river incision, i.e. erosion of underlying rock or remobilization of sediment (**Fig. 3e1**; Allen and Densmore, 2000; van den Berg van Saparoea and Postma, 2008; Armitage et al., 2011, 2013, 2018b; Tofelde et al., 2019; Zhang et al., 2020). This pattern in the $Q_s$ response can be observed at individual locations along the channel (**Fig. 3d1**), but also at the catchment outlet as an integrated signal of the entire catchment area (**Fig. 3e1**, sampling location indicated by yellow star). The amount of change in $Q_s$ differs with location. For example, an increase in $Q_w$ causes greater incision and higher $Q_s$ peaks upstream compared to downstream. In contrast, a step increase in tectonic uplift (base level fall) will generate a delayed, but sustained increase in $Q_s$ at the basin outlet (**Fig. 3e2**; Bonnet and Crave, 2003; Armitage et al., 2011; Zhang et al., 2020). This sustained increase in $Q_s$ can be observed at different locations along the channel, but occurs at different times as it is related to the upstream migrating knickwave (**Fig. 3d2**).

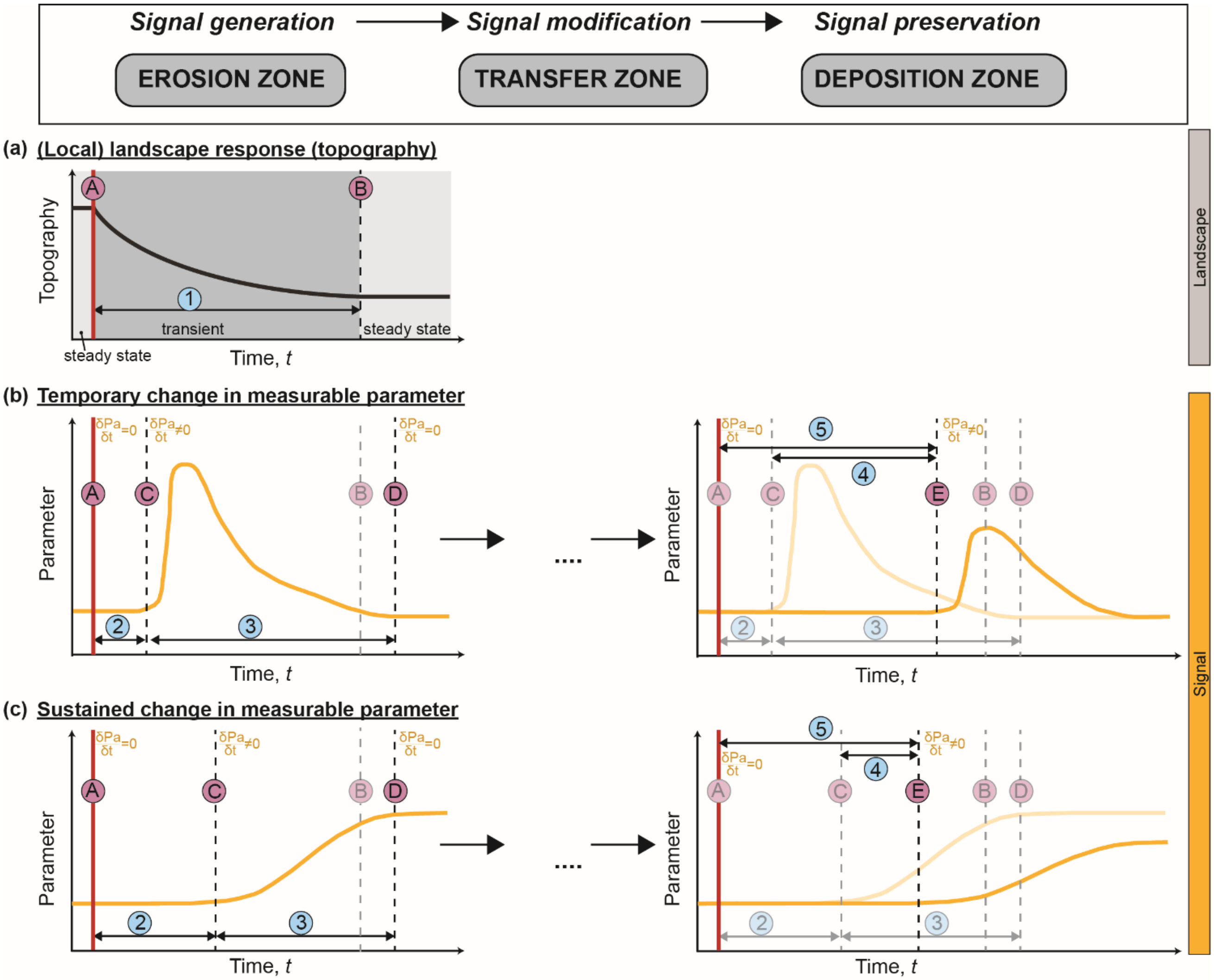


**Distinct moments in time**
(A) Time of change in boundary conditions (external perturbations)
(B) End of transient landscape adjustment phase
(C) Onset of signal generated in the source area ($\delta$Parameter/$\delta$t ≠ 0)
(D) End of signal generated in the source area ($\delta$Parameter/$\delta$t = 0)
(E) Signal arrival in the deposition area ($\delta$Parameter/$\delta$t ≠ 0) = signal arrival time

**Periods of time**
(1) **Landscape response time (A-B)**: Time of externally forced topographic landscape adjustment (synonyms: equilibrium or adjustment time)
(2) **Signal onset time (A-C)**: Time until a measurable change in the parameter of interest in the source is generated ($\delta$Parameter/$\delta$t = 0 or dominated by a previous adjustement)
(3) **Signal duration time (C-D)**: Time of a measurable change in the parameter of interest in the source ($\delta$Parameter/$\delta$t ≠ 0)
(4) **Signal transfer time (C-E)**: The time required for the signal to travel to the deposition zone
(5) **Total signal lag time (A-E)**: Time between change in boundary conditions and onset of measurable change in the parameter of interest in the deposition zone ($\delta$Parameter/$\delta$t = 0)

***Figure 4*** *Different types of ‚times‘ applicable to signals generated within and transported to different segments of SRSs. Changes in boundary conditions cause a topographic response in the landscape (a) and the generation of signals (b and c). Signals are a change in any measurable sedimentary parameter of interest. The change can be of temporary (b) or sustained (c) nature. For both topographic and sediment parameter changes certain times can be defined. We distinguish between distinct moments in time (letters) and periods of times (numbers). For detailed explanations on the different types of time see main text.*

### 3.2.1 Times related to signal generation

For any kind of environmental signal, specific signal related times can be distinguished (**Fig. 4**). We differentiate between distinct moments in time (vertical lines and letters) and periods of time (horizontal arrows and numbers). After a change in boundary conditions (A), the landscape responds by adjusting its topography until steady state conditions are achieved again (B**; Fig. 4a).** The required time is referred to as *landscape response time* **(1; see section 3.1).** Adjustments of the landscape generate signals, i.e. measurable changes in certain sediment parameters (**Fig. 4b and c**). In the context of signal generation, we present and discuss the following two signal related time periods: the *signal onset time* (2) and the *signal duration time* (3).

**We define the *signal onset time* (2) as the time period between the onset of a change in boundary conditions and the onset of change in a sediment parameter (C).** The *signal onset time* is equivalent to the sediment flux lag time by Li et al. (2018a), who investigated numerically how long expected increases or decreases in $Q_s$ lag behind periodic step changes in uplift rates. They found that *signal onset times* increase the farther the landscape was from steady state prior to the change in boundary conditions (Li et al., 2018a), which is particularly important for cyclic climate fluctuations (e.g. Milankovitch-driven climate changes). In addition to prior landscape state, *signal onset times* depend on the parameter of interest. For example, an increase in uplift rates and tectonic activity might affect the grain size distribution in fluvial sediments relatively fast, while it takes longer until this change becomes detectable in samples for detrital thermochronology (e.g., Whittaker et al., 2010).

Once a signal is generated, it persists until the parameter attains a stable value again (D). Hence, **we define the *signal duration time* (3) as the time period characterized by a measurable change in a sediment parameter ($\delta_{\mathrm{Parameter}}/\delta t \neq 0$).** Sharman et al. (2019) used *signal response times* to describe the time until a sediment parameter attains within a certain percentage of its new, steady value. The *signal duration time* as we define it lasts at least as long as the transient landscape response phase, and potentially beyond. Consequently, during *signal duration times* fluvial sediments carry mixed information from parts of the landscape adjusted to prior and to new conditions. Only once the parameter is fully adjusted to new steady conditions (end of signal duration D), the parameter represents current conditions within the landscape. For example, the $^{10}$Be concentration in fluvially transported sediments are regularly applied as a proxy to estimate catchment averaged denudation rates (Balco and Stone, 2005; Charreau et al., 2011; Mandal et al., 2015; Puchol et al., 2017; Mariotti et al., 2019). A theoretical step change in a catchment averaged denudation rate causes an exponential adjustment in detrital $^{10}$Be concentrations. Hence, during the period of $^{10}$Be adjustment, the denudation rate calculated from $^{10}$Be in detrital sediments differs from true denudation rates (Willenbring et al., 2013; Garcin et al., 2017; Mudd, 2017; Mason and Romans, 2018). Hence, if boundary conditions change at a period shorter than parameter-specific *signal onset* (2) and *signal duration times* (3), the measured parameter never represents current landscape conditions. However, it does not mean that no signals are generated nor that no information can be extracted from sediment signals. Signals, as we define them, are particularly generated during landscape transience, and hence can be used to identify times of environmental changes. Quantitative reconstructions of true current landscape conditions, however, are limited to times when the measured parameters are constant throughout the time period of interest.

### 3.2.2 Times related to signal transfer

Signals are typically generated in mountainous areas where sediment is produced (erosion zone). To be preserved in sedimentary archives, the signal carrying sediments need to be transported along SRSs to their deposition zone, which requires time. In addition, signals do not only take time to be transported along SRS, but also may be modified in their shape (amplitude, phase) or even destroyed during transport due to threshold behavior in sediment transport processes, storage and recycling of sediments in floodplains, or feedback mechanisms with the fluvial system (Jerolmack and Paola, 2010; Simpson and Castelltort, 2012; Armitage et al., 2013; Godard et al., 2013; Braun et al., 2015; Romans et al., 2016; Straub et al., 2020). The modification of a signal is indicated in **figure 4** (transparent vs. solid yellow curves), but will not be further addressed here (short discussion in section 5). Instead, we focus on the times that are important for reconstructions in cases when signals have reached the sink. In the context of signal transfer, we present and discuss the following two signal related time periods: the *signal transfer time* (4) and the *total signal lag time* (5).

When reconstructing past conditions from sedimentary archives, the arrival time of the first measurable change of a parameter in the deposition zone (E) (which can be continental or marine) is important. **We define the *signal transfer time* (4) as the time between the onset of signal generation in the source (C) and the *signal arrival time* in the sink (E).** *Signal transfer times* are expected to vary with the parameter of interest (due to grain size dependent differences in transport mode) and from archive to archive (due to differences in catchment size and hydraulic conditions). Consequently, an individual local change in boundary conditions can result in different times of a first detectable parameter change in the sink, as well as in differences in signal duration (e.g., Ramisch et al., 2018).

**Moreover, we define the *total signal lag time* (5) as the total time between the change in boundary conditions (A) and the signal arrival in the sink (E).** The *total signal lag time* is the sum of the *signal onset time* (2) and the *signal transfer time* (4). Oftentimes, studies refer to the *total signal lag time* simply as lag time (Goodbred and Kuehl, 2000; Goodbred, 2003; Covault et al., 2010; Duller et al., 2019). For example, the Paleocene-Eocene boundary is characterized by a global warming event with an abrupt onset referred to as the Paleocene/Eocene Thermal Maximum (PETM), defined by an abrupt negative excursion in soil carbon isotopes, $\delta^{13}C$ (McInerney and Wing, 2011). Studies from the central US (Foreman et al., 2012; Foreman, 2014) and the Spanish Pyrenees (Schmitz and Pujalte, 2003, 2007; Chen et al., 2018) have related extensive sheets of coarser fluvial sediments during the PETM to increased seasonal precipitation, despite overall drier climate conditions. Duller et al. (2019) quantified the *total signal lag time* between the onset of the PETM and the onset of coarse-grained sediment deposition in the terrestrial realm, as well as the onset of increased terrestrial input in the marine realm. They found *total signal lag times* of ~16 kyr in both proximal nonmarine and distal deep-marine sites separated by ~300 km distance.

In summary, signals are initiated during transient landscape response and can be transported through the SRS and arrive in the sink (E) even before the characteristic *river response time* has passed (B), such that the *total signal lag time* (5) can be shorter than the *river response time* (1) (**Fig. 4**, Shen et al., 2012; Straub et al., 2020). These signals indicate changes in boundary conditions and are not representative of steady state conditions. It is the generation of a sediment parameter change, its transport and the archiving during this transient state that are poorly understood, but hold high potential for rapid imprint of environmental changes in the stratigraphic record.

We argue that *signal transfer times*, and hence *total signal lag times*, which are of particular importance for reconstructions from sedimentary archives, greatly depend on the hydraulic characteristics of the sediment fraction the parameter (signal) is measured on (= *hydraulic grain size fraction*). Therefore, in **section 4**, we discuss which parameters impact *signal transfer times* and how *signal transfer times* vary with *hydraulic grain size fractions*.

## 4 Parameters affecting signal transfer time

*Signal transfer times* describe the required time for the signal containing sediment fraction to be transported from the source to the sink. We think that sediment transport times, and thus *signal transfer times*, are governed by two main factors summarized in **figure 5**: (1) the fraction of time a sediment particle is in motion vs. immobile within the active channel and (2) the probability of transient sediment storage outside the active channel. Fast sediment transport or short *signal transfer time* (dark colors in **Fig. 5**) is the result of high grain mobility and low transient storage probability, whereas dominantly immobile grains and high storage probability result in long transport times (light colors in **Fig. 5**). Both, the fraction of time in motion and the storage probability, depend on a range of factors, which will be discussed separately for the terrestrial and marine realm. Some of those factors vary greatly with *hydraulic grain size fractions* (blue), while others are less dependent on *hydraulic grain size fractions* (grey). In the following two sections (**sections 4.1 and 4.2**), we will discuss (1) how each factor in **figure 5** relates to short or long *signal transfer times*, (2) the grain size dependency of the factor, and (3) drivers that control the specific factor.

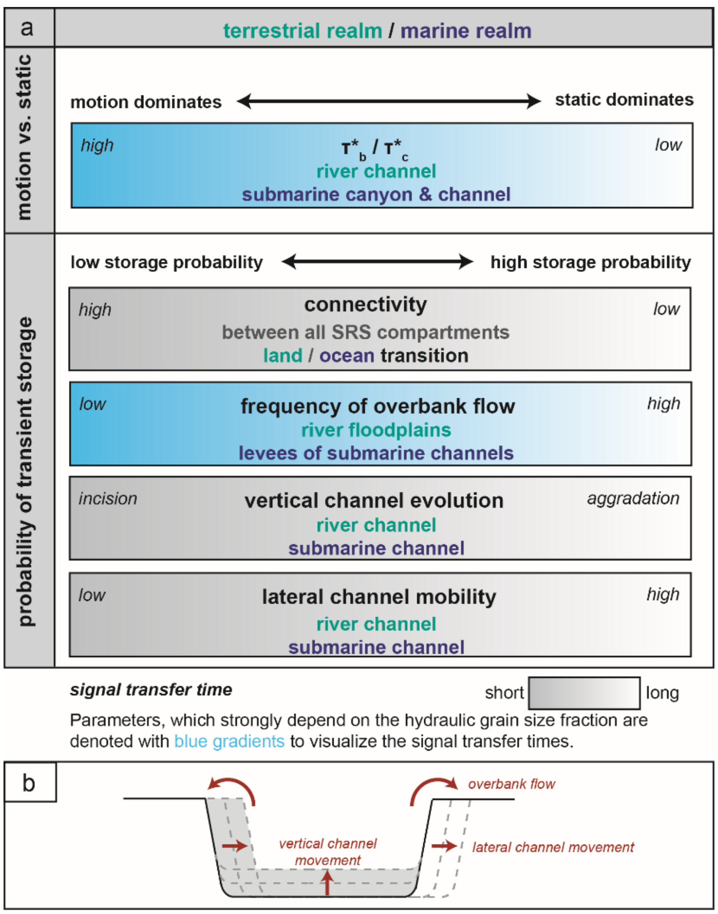


*Figure 5 Schematic summary of factors influencing sediment transport times in channelized systems and, hence, signal transfer times. (a) Signal transfer times depend on the fraction of time a grain is in motion versus immobile within the active channel, and the probability of storage outside the active channel. Both, the time in motion and probability of storage, depend on a range of factors, which themselves range between endmembers as indicated in italics. Accordingly, the signal transfer times range from short (dark colors) to long (white colors). Factors that vary greatly with hydraulic grain size fraction are marked in blue, factors that vary less between grain sizes are shown in grey. Green and blue font indicates the locations where these factors apply in the fluvial and marine realm, respectively. (b) Schematic summary of channel evolution terms.*

### 4.1 Times of sediment in motion vs. static

In the simple case of a spatially fixed, single-thread river channel with no overbank flow, the required transport time of a certain sediment particle is determined by the fraction of time the grain is mobile versus immobile within an active channel. Particle motion on land is initiated and persists, if the vertical component of driving forces (fluid shear and lift) exceed the retaining forces (gravity and friction) (Wiberg and Smith, 1987). In practice, on the reach scale this is often estimated by the Shields criterion in which the bed shear stress, $\tau_b$ [N m$^{-2}$], exerted by the fluid on the channel bed exceeds the critical shear stress for initiation of motion, $\tau_c$ [N m$^{-2}$], such that (Shields, 1936; Parker et al., 2003; Zanke, 2003; Van Rijn, 2007):

$$\tau_b > \tau_c \quad \text{(eq. 2).}$$

Oftentimes, shear stresses, $\tau$, are compared in a non-dimensional form. This allows the direct comparison of driving forces of sediment motion ($\tau$) with resisting forces (grain diameter, $D$ [m], and grain density, $\rho_s$ [kg m$^{-3}$]). The non-dimensional form of shear stress, $\tau*$ or $\theta$ [-], is called the Shield's parameter or Shield's criterion (Shields, 1936) and is defined as:

$$\tau^* = \frac{\tau}{(\rho_s - \rho_w)gD} \quad \text{(eq. 3),}$$

where $\rho_w$ [kg m$^{-3}$] is the density of water and $g$ [m s$^{-2}$] the acceleration due to gravity. Combining equations 2 and 3 yields that grains entrain when the bed Shields parameter exceeds the critical Shields parameter:

$$\tau_b^* > \tau_c^* \quad \text{or} \quad \frac{\tau_b}{(\rho_s - \rho_w)gD} > \tau_c^* \quad \text{(eq. 4).}$$

The bed shear stress can be approximated for rivers experiencing steady, uniform flow in a channel whose width is much greater than its depth as (e.g., Tucker and Slingerland, 1997):

$$\tau_b \approx \rho_w g h S \quad \text{(eq. 5),}$$

with $h$ [m] being the flow depth and $S$ [-] the channel gradient. Combining equations 4 and 5 yields:

$$\frac{\rho_w h S}{(\rho_s - \rho_w)D} > \tau_c^* \quad \text{(eq. 6).}$$

$\tau_c^*$ has been shown to vary little among many rivers (~0.03 to 0.06) and is therefore often considered as constant for a given site (e.g., Meyer-Peter and Müller, 1948; Buffington and Montgomery, 1997; Wilcock et al., 2003). If $\tau_c^*$ is treated as a constant, equation 4 indicates that in theory small grains with low densities are more mobile than coarse grains as they require lower bed shear stress to move. However, while this might work for equally sized sediments, the relationship gets more complicated in grain size mixed sediments due to the hiding-exposure effect (Parker et al., 1982; Wilcock and Crowe, 2003; Pfeiffer and Finnegan, 2018). The hiding-exposure effect describes that small grains can be protected from the initiation of motion when they hide in pockets between larger grains, thereby increasing the critical shear stress to initiate grain motion. In contrast, coarse grains surrounded by fine grains can protrude further from the bed into the water column than the fine grains and are exposed to increased drag, thereby decreasing the critical shear stress of initiation of motion. In addition, further studies indicate that $\tau_c^*$ cannot simply be regarded as a constant, especially for steeper rivers (S>5%), because $\tau_c^*$ varies, for example, with channel slope (Lamb et al., 2008; Recking et al., 2009;

Scheingross et al., 2013; Prancevic and Lamb, 2015), previous flow conditions (Turowski et al., 2011; Masteller et al., 2019), or sand content (Wilcock and Crowe, 2003; Curran and Wilcock, 2005; Lamb et al., 2008; Houssais and Lajeunesse, 2012). Hence, $\tau_c^*$ of a grain size range is better represented by a probability distribution instead of a single value (Kirchner et al., 1990).

Motion initiation on clay-sized particles may in addition be hindered by cohesion effects (e.g., Hjulstrom, 1955), as $\tau_c^*$ of cohesive sediment mixtures exceed $\tau_c^*$ of size-equivalent cohesionless sediments by a factor up to 50 (Kothyari and Jain, 2008). Several sediment parameters are measured on clay-sized material (Hessler and Fildani, 2019), for example the Chemical Index of Alteration (CIA; Nesbitt and Young, 1982), which is commonly used as a proxy for degree of chemical weathering in the sediment generation zone. The small and often flake-shaped particles have low settling velocities (Dietrich, 1982) and, hence, require low flow velocities for their further transport. However, when being transiently stored, *transfer times* of signals bound to clay-sized material will be prolonged due to hindered erosion caused by cohesion effects.

Generally, sediments transported in suspension will travel at the same speed as water. At a first order, the travel speed of water is ~1m $s^{-1}$, resulting in ca. 90 km per day. Hence, if transported without any deposition, suspended sediments would reach the ocean in a 1000 km long river in less than two weeks. On the contrary, bedload sediments travel by intermittent transport, with periods of deposition on the river bed. Kooi and Beaumont (1994) introduced the idea that a local rate of deposition (within a river channel) can be described as inversely proportional to a transport length. The transport length describes the distance a grain can travel with the flow prior to deposition on the river bed. The transport length exerts a strong control on the river morphodynamics and thus on the *signal transfer times* (Davy and Lague, 2009; Bradley and Tucker, 2012; Ganti et al., 2014; Kasprak et al., 2015). In fact, numerical studies showed that large transport lengths behave like detachment-limited systems, while small transport lengths behave like transport-limited systems (see section 3.1, Kooi and Beaumont, 1994; Davy and Lague, 2009). Recently, a new formalism for this transport length was introduced and allows for field estimations of this parameter (Guerit et al., 2019). The authors concluded that 2/3 of their studied sites tend toward a transport-limited behavior. This implies that even in the absence of massive storage (see section 4.2), a majority of sedimentary systems do not export their sediments instantaneously.

In summary, for a fixed channel geometry, the fraction of time the critical shear stress for a certain *hydraulic grain size fraction* is exceeded and particles are in motion depends on river geometry, degree of sediment sorting, and the discharge conditions of the river. Not only the total amount of discharge plays a role for sediment motion, but also the distribution of discharge through time, e.g. its seasonality or the frequency and magnitude of flooding events (Haynes and Pender, 2007; Masteller et al., 2019). But as a general rule of thumb, the higher the bed shear stress (deeper and steeper channels, **eq. 5**), the more often particles of a certain grain size are in motion. Small particles are generally more frequently mobile than coarser particles, and transport times consequently shorter. In rivers with mixed grain sizes, these relationships become more complicated due to, for example, hiding exposure effects.

In the context of channelized systems in the marine realm, grains will also be entrained when $\tau_b > \tau_c$ (**Fig. 5a**). However, while on land the bed shear stress acting on the sediment on the bed is mainly exerted by the overlying water column (**eq. 5**), the bed shear stress in marine channels largely depends on the character of sediment gravity flows (such as turbidity currents) within submarine canyons and channels (Piper, 1970; Cossu and Wells, 2012; Talling, 2014). Turbidity currents have the ability to erode sediments from the seafloor, if they are moving fast enough so that their bed shear stress, $\tau_b$, exceeds the critical value, $\tau_c$, of the sediment on the seafloor, a process known as autosuspension and self-acceleration (e.g., Heerema et al., 2020). Laboratory experiments and direct monitoring of turbidity currents have shown that turbidity currents are highly stratified and their basal layer is characterized by the highest sediment concentrations (Cossu and Wells, 2012 and references therein; Paull et al., 2018). The bed shear stress in this dense basal layer determines whether erosion occurs at the seafloor. The bed shear stress depends on the dynamic viscosity, $\mu$ [N s m$^{-2}$], the eddy viscosity, $\kappa$ [N s m$^{-2}$], and the turbidity current velocity, $u$ [m s$^{-1}$] (e.g., Stacey and Bowen, 1988):

$$\tau_b = (\kappa + \mu)\,\frac{\partial u}{\partial z} \qquad \text{(eq. 7)},$$

and be transformed to a dimensionless term $\tau_b^*$ according to **equation 3**. The probability of $\tau_b^* > \tau_c^*$ will be highest, where turbidity currents occur at high frequency, carry large volumes of sediment and coarse grain sizes, and in a setting of high confinement (synonyms: channelization or topographic roughness), such as deep submarine canyons and channels.

## 4.2 Probability of transient storage

In addition to times of no sediment transport within a confined channel due to flow conditions not exceeding the initiation of sediment motion on the river bed or sea floor, *signal transfer times* can be increased due to sediment storage along the SRS outside of the active channel. The concept of SRS connectivity describes sediment transfer from all potential sources to all sinks through different geomorphic segments of the SRS and can be used to describe the continuity of mass transfer in a SRS (Hinderer, 2012; Fryirs, 2013; Bracken et al., 2015; see Najafi et al., 2021 for a recent review). A high degree of connectivity (**Fig. 5a**) allows fast sediment and signal transfer, while a low degree of connectivity results in sediment storage within different segments of the SRS (hillslope, fluvial system, shelf, continental slope, deep marine basins). On land, sediment can be stored due to reduced connectivity on hillslopes (**Fig. 1**; DiBiase and Lamb, 2013; Hoffmann, 2015) and within the river system. Once in the river, sediment particles can end up outside of the active river channel in form of (1) floodplain deposition due to overbank flow, (2) burying in the channel bed due to sediment deposition during periods of channel aggradation, and (3) deposition due to lateral channel movements (e.g., point bar accretion) (**Fig. 5a&b**).

First, during floods causing overbank flow, sediments can be washed onto the floodplain, where they can remain for long times before remobilization (**Fig. 1;** Wittmann et al., 2011, 2020). The likelihood of being deposited on the floodplain due to overbank flow, in turn, varies with the mode of transport. Fine particles, including sand, silt, and clay, generally travel in suspension in the water column (Shields, 1936) and are more likely to be deposited on the floodplain during overbank flow conditions. In contrast, coarse particles, such as gravel, are usually transported as bedload (Shields, 1936) and therefore remain within the channel bed even during overbank flow conditions. Consequently, gravel has a lower probability of being washed onto floodplains (Malmon et al., 2003).

Second, storage probability is increased if rivers are in a phase of aggradation and, hence, deposit sediments in their beds (**Fig. 5b**). Transport-limited rivers respond with sediment deposition along the channel to steepen their slope, for example following a decrease in upstream water discharge or an increase in upstream sediment supply (e.g., van den Berg van Saparoea and Postma, 2008; Armitage et al., 2013; Tofelde et al., 2019). Alternatively, base level rise leads to sediment deposition along the channel (e.g., Blum and Törnqvist, 2000). Deposited sediments will only be remobilized if boundary conditions change from channel aggradation to channel incision, which can be triggered, for example, by base level lowering, increase in water discharge, or reduced sediment supply (Allen and Densmore, 2000; van den Berg van Saparoea and Postma, 2008; Armitage et al., 2013; Tofelde et al., 2019).

Third, sediment gets stored due to lateral channel movement (**Fig. 5b**). Sediments of all grain size fractions can be deposited when the active channel moves sideways either through avulsion (Slingerland and Smith, 2004; Jerolmack and Mohrig, 2007) or by gradual sideways migration and associated accretion of barforms (Einstein, 1926; Hickin and Nanson, 1984; Bufe et al., 2019). However, it should be noted that lateral channel mobility can also remobilize previously deposited sediments. Therefore, lateral channel mobility increases the storage probability of sediments in motion within the active channel, but decreases the storage probability of previously deposited sediment. Both the lateral and vertical movement of the active channel result in potentially long-term sediment incorporation in floodplains (Nakamura and Kikuchi, 1996; Wittmann et al., 2011, 2020; Bradley and Tucker, 2013; Coulthard and Van De Wiel, 2013), alluvial fans (Jolivet et al., 2014; D'Arcy et al., 2015, 2017; Guerit et al., 2016; Mason and Romans, 2018; Carretier et al., 2020), fluvial terraces (Blöthe and Korup, 2013; Limaye and Lamb, 2016; Schildgen et al., 2016; Malatesta et al., 2017, 2018; Tofelde et al., 2017; Quick et al., 2019), or entire valley fills (Hilley and Strecker, 2005).

In the ocean, sediment can be stored proximal on the shelf (Miller and Kuehl, 2010) and more distal in submarine canyons (Brocheray et al., 2014; Maier et al., 2019). The *signal transfer time* at the land-ocean interface depends on the degree of connectivity between these SRS segments. At high connectivity grains can travel unhindered through the entire SRS and are discharged directly into the submarine canyon and onto the marine basin floor (Romans et al., 2009; Covault and Graham, 2010; Bernhardt et al., 2017; Blum et al., 2018). Although a high degree of connectivity between any segment of SRSs reduces *signal transfer times*, the connectivity at the land-ocean transition is of particular importance. Whereas shelves have traditionally been seen as transient sedimentary sinks, several studies have recognized that shelves can act as fast conveyors of sediment from land to the deep ocean, if canyon heads are incised across continental shelves and tap into coast-parallel sediment transport (the ocean littoral cell) or are connected to a river mouth (**Fig. 1**; Walsh and Nittrouer, 2003; Covault and Graham, 2010; Bernhardt et al., 2015), if terrigenous sediment supply is high enough to cause delta migration to the shelf edge (Burgess and Hovius, 1998; Carvajal and Steel, 2006), or if coast-parallel bottom currents sweep sediment off the shelf edge or into submarine canyons (Bernhardt et al., 2016). Hence, signal propagation to deep-marine submarine fans is most efficient when connectivity is high, which in many (but not all) systems is enhanced during sea level lowstand, because river mouths extend to the shelf edge and discharge directly into slope canyons (Blum et al., 2018). In contrast, in systems that are disconnected (e.g., during current high sea-level conditions and, thus, increased accommodation space on the shelf), many sediment density flows die out in the upper reaches of the marine SRS (Heerema et al., 2020), leading to intermediate storage of sediment on the shelf, along canyons and channel-levee systems, which may reach the final sediment archive only after remobilization by stronger flows. Regarding signal manifestation in the sediment sink, the role of system connectivity can be complex. Along the Chile margin, Bernhardt et al. (2017) compared the onset of deglacial aridification in marine sedimentation patterns offshore river basins located along a gradient in SRS connectivity. Aridification decreased sediment supply and turbidite frequency with no resolvable *total signal lag time* in all studied catchments. However, similar signals in the sinks are due to distinct underlying causes ranging from high SRS connectivity to abrupt connectivity loss.

In the distal part of a marine SRSs, sediment can be buried within the bed of submarine channels or their overbank levees due to (1) frequency of overbank flow or, in other words, frequency of overspill of the turbidity current onto adjacent levees, (2) burial in the channel bed (vertical channel movement), and (3) lateral channel movement (**Fig. 5**). First, turbidity currents form large clouds of suspended sediment that can be several 10s of meters (Azpiroz-Zabala et al., 2017) to several 100s meter in height (Völker et al., 2008). Superelevation induces the diluted (fine-grained) upper sediment cloud of the turbidity current to spill over and deposit sediment onto the levees while eroding, bypassing and/or depositing within the channel itself, a process known as spillover and flow-stripping, which is especially efficient at meander bends (Normark et al., 1980; Piper and Normark, 1983; Fildani et al., 2006; Straub and Mohrig, 2008). Second and third, although the dynamics and frequencies of lateral (avulsion and lateral migration) and vertical (incision vs. aggradation) submarine channel movements differ from terrestrial rivers (e.g., Jobe et al., 2020), the general effect of lateral and vertical submarine channel movement on sediment transport times should be analogous to terrestrial river dynamics explained above.

Taken all factors together, the *signal transfer time* of a SRS over timescales longer than decades is therefore a composite of event-scale hydraulic transport dynamics combined with time-averaged storage probability (**Fig. 5**). Because *signal transfer times* depend on several different factors (**Fig. 5**), they are far from trivial to predict and notoriously difficult to measure. In the following section, we review promising approaches to quantify sediment transport times.

### 4.3 Quantification of sediment transport times

Quantification of sediment transport time is not straightforward as it requires the determination of the velocity of a grain at various scales: from motion within an active channel to motion at the scale of the whole SRS, including times of transient storage. In this section, we focus on methods developed to measure the total transport time of sediment.

Short-lived radionuclides (e.g., $^{234}$Th, $^{7}$Be, $^{210}$Pb, $^{137}$Cs) can be used to quantify timing of fine-grained sediment dispersal along SRSs over short timescales ($10^0$-$10^2$ yr) (Zapata and Nguyen, 2009; Du et al., 2012). Malmon et al. (2005) showed that the fine-grained fraction can pass through a fluvial valley of 5 km length within hours and only 14% of the fine sediment in floods is predicted to be deposited on the floodplain. Similarly, fine-grained fluvial flood sediments of the Eel River were dispersed widely over the shelf and continental slope to about 500 m water depth in one month (Sommerfield and Nittrouer, 1999). Direct tracing of gravel transport using integrated transponder tags is only applicable to the gravel grain size fraction and on short timescales (Lamarre et al., 2005). Applying this method, among others Bradley and Tucker (2012) recorded mean and maximum travel distances of ~100 m and ~700 m, respectively, over 3.5 yr.

At longer timescales (>$10^3$ yr), uranium-isotope series are frequently used on small grains (<63 microns) to determine a 'comminution age' of the sediment, which refers to the time elapsed between the generation of the silt-sized sediment grain by comminution of bedrock and its deposition (DePaolo et al., 2006). The sediment transport time refers to the time difference between the comminution age and its depositional age (Chabaux et al., 2006; DePaolo et al., 2006; Li et al., 2016). Following this approach, Suresh et al. (2014) demonstrated that the small grains of the large and tectonically stable Murrumbidgee River catchment (Australia) are stored for ~200 kyr on hillslopes before they can reach the river network and be evacuated from the catchment area. Using the same method, Li et al (2016) quantified the transport time of the sediments deposited in the Okinawa Trough (East China Sea), which is mainly fed by the Yangtze River and by sediments coming from Taiwan. They documented transport times on the order of 100 to 200 kyr. Moreover, DePaolo et al. (2006) measured sediment-transport times to a deep-marine site with depositional ages <1 Ma using uranium isotope ratios ($^{234}U/^{238}U$) and observed times ranging between 10 kyr up to 400-600 kyr with uncertainties of ±40 to

±100 kyr for siliciclastic silt-sized sediment. Hence, even fine-grained sediment may display very long transport times to the deep sea due to intermediate storage in soils, floodplains and shelves and redistribution on the seafloor (DePaolo et al., 2006; DePaolo, 2012).

Analyzing the concentration of several cosmogenic nuclides in the modern sediments of the Murray-Darling basin (Australia), Fülöp et al. (2020) concluded that successions of burial and remobilization led to a total transport time of more than 1 Ma. Similarly, Dosseto et al. (2006) showed that the suspended load issued from the Andes and traveling through the Amazon basin is temporarily stored within the foreland basin for ~5 kyr. For the coarse-grained fraction, Sinclair et al. (2019) documented recycling of pebbles deposited 5 Ma ago based on detrital cosmogenic $^{21}$Ne concentrations. The duration of sediment storage outside the active channel can also be measured from the ratio of cosmogenic meteoritic $^{10}$Be over $^{9}$Be within sediments (Wittmann et al., 2015). Repasch et al. (2020) tested this method along the Rio Bermejo (Andean foreland basin, northern Argentina) and observed that the suspended load travels ~1200 km from sources to sink in 8.4±2.2 kyr. Within the Indus SRS, Clift et al. (2008) suggests based on Nd composition on a limited set of samples, that the clay-sized fraction travels as suspended load rapidly through the system after an increase in monsoon strength with no resolvable lag time, while the bedload transport is decoupled from the suspended load and heavy mineral (zircon) grains travel about of 7–14 kyr from source to sink (Clift and Giosan, 2014). A new tool for quantifying sediment transport times is being developed using subaqueous bleaching rates of optically stimulated luminescence (OSL) in quartz and feldspar. Observations indicate that grains progressively bleach during transport, making the degree of bleaching a potential tool for measuring sediment transport times (Gray et al., 2017).

Rather than measuring the time during which the sediment has been stored, Carretier and Regard (2011) demonstrated that the concentration in terrestrial cosmogenic nuclides of boulders can be used to determine the rate of transport of a grain, when abrasion is limited. Building on this approach, Carretier et al. (2019) measured the $^{10}$Be concentration of gravels originating from the same outcrop in the Central Andes and showed that the coarse grains are transported at different rates on millennial time scales. This study provides field evidence that sediment can be stored for a substantial amount of time on their way to the sedimentary basins simply by the way rivers transport sediments.

Finally, numerical landscape evolution models can bring insights on the dynamic of sediment export from sources to sinks. Carretier et al. (2020) showed with numerical simulations that even in a landscape at steady state, some pebbles can be stored within a piedmont for a period of time substantially longer than the average population of sediments. In their specific numerical setup, most of the grains leave the piedmont after 400 yr, but ~5% stay there for ~1 Ma. This is in line with the field study of Phillips et al. (2007), who observed in New Zealand that grains can be stored within terraces for at least 100 yr, but that 50% of the stored sediments will remain for more than 2000 yr.

In summary, the storage and remobilization of sediments on their way to the depositional segment may be a major source of complexity to unravel climatic and tectonic events within sedimentary archives and this is why accurate methods to quantify the transport time of the sediments from sources to sinks are deeply needed.

## 5 Preservation of catchment signals in stratigraphy

Environmental reconstructions from sedimentary deposits require a detailed understanding of signal modification during transport along SRSs, as well as of signal preservation in stratigraphy. As it is beyond the scope of this manuscript, we only briefly summarize processes of signal modification and refer the reader to further literature. We then focus particularly on the preservation of signals in stratigraphy with an emphasis on signals that originate in the catchment.

After signal generation in the source the signal can still be modified or even lost during transport along SRSs (modification indicated by transparent vs. solid yellow curves in **Fig. 4**). Signals can be modified due to (1) autogenic fluctuations in sediment transport rates, (2) transient sediment storage along SRSs, (3) sediment abrasion during transport and, (4) mixing with sediments from other source areas prior to deposition (=dilution). First, sediment transport rates in rivers undergo autogenic (self-organized) fluctuations, which have been related to threshold behavior in sediment transport processes (Muto and Steel, 2001; Coulthard and Van De Wiel, 2007; Clarke et al., 2010; Jerolmack and Paola, 2010; Van De Wiel and Coulthard, 2010; Hajek and Straub, 2017; Guerit et al., 2020). As a consequence, autogenic transport fluctuations destroy a signal (Jerolmack and Paola, 2010), or interfere with a certain frequency of input signals (Paola and Foufoula-Georgiou, 2001; Paola, 2016). Hence, there are processes in the depositional SRS segment that are unrelated to the signal of interest, but may modify the expression of that signal (for a recent review see Scheingross et al., 2020). Second, storage and remobilization of a sub-fraction of sediment (**section 4.2**), for example in the channel bed itself, floodplains, fluvial terraces, alluvial fans or entire valley fills, can cause a change in signal phase and amplitude (Romans et al., 2016 and references threin). Third, during transport grains are size-reduced by abrasion (Lewin and Brewer, 2002; Attal and Lavé, 2006, 2009; Olen et al., 2015; Dingle et al., 2017; Lupker et al., 2017), which includes processes like attrition (pebbles scraping against each other), splitting, breaking or chipping. Hence, grains might fall into a smaller *hydraulic grain size fraction* during transport and/or experience an alteration of their shape or composition (e.g. $^{10}Be$ concentration). Fourth, signals can be diluted when mixed with hydraulic grain size equivalents from another source, carrying a different or no signal (Attal and Lavé, 2006). For more detailed reading on signal modification, we refer to reviews by Romans et al. (2016) and Allen (2017).

In cases where a signal arrives in the sink, it needs to be preserved and measurable in the stratigraphic record to be applicable for environmental reconstructions. Here, we consider how the dynamics associated with the development of the stratigraphic record may impact the preservation of signals and, thus, our ability to accurately reconstruct them from the record. In this context, we are assuming that signals have not been completely obscured by the processes mentioned above, but have been transmitted to the depositional segment. We first discuss the arrival times of several signals related to a single change in boundary conditions, and second stratigraphic completeness and fidelity. A stratigraphic section is considered 'complete' when it does not encompass hiatuses longer than the time interval of successive sampling (Sadler, 1981), whereas stratigraphic fidelity refers to the ability of a sediment archive to record the rate of geomorphic or geologic processes at the time scale of interest (Kemp, 2012).

## 5.1 Signal arrival times

As previously discussed, we suggest grouping sediments by *hydraulic grain size fractions* when investigating environmental signal reconstruction from stratigraphy. Consider a simple hypothetical scenario where *hydraulic grain size fraction* is directly related to *signal transfer time* such that fine-grained sediment transmits catchment signals quickly, whereas signals associated with coarse-grained sediment are comparably slower (Carretier et al., 2020; Watkins et al., 2020). The implication is that the onset of the signal of interest in fine-grained parameters would be at a lower stratigraphic position compared to parameters associated with coarse-grained sediment for the same change in boundary conditions (**Fig. 6**). Thus, what might appear as a prolonged environmental change in the stratigraphic record would actually be the manifestation of different grain size-dependent *signal transfer times*.

However, this simple scenario does not consider the additional effects related to probability of transient storage. For example, in SRSs that are characterized by significant transient storage of fine-grained sediment (e.g., in floodplains), the arrival of the signal as a function of *hydraulic grain size fraction* would be more complex as a consequence of segment connectivity, channel mobility, and other aspects depicted in **figure 5**.

An analysis of the composition of the fine-grained sediment fraction (Nd and Sr isotopes of mud to fine sand) in the Indus submarine canyon by Li et al. (2018b) showed that modern submarine canyon sediment reflects the isotopic composition of the river sediment (**Fig. 1**). However, the U-Pb signature of detrital zircons in the coarse silt to fine sand fraction does not mirror the river sediment composition (Li et al., 2019). Hence, in such a system, a potential signal may be transferred rapidly within the geochemical composition of the fine-grained fraction, but may be stuck in the terrestrial intermediate storage when the geochemical signal in the silt to sand-sized heavy mineral fraction is considered. Therefore, different transport times of mud and zircons may result in an offset of *signal arrival times* in the stratigraphic record (**Fig. 6B**). Studies characterizing parameters such as sediment geochemistry as a function of grain size (e.g., Jonell et al., 2018) suggest that bulk geochemical composition as a source-area indicator could be misleading.

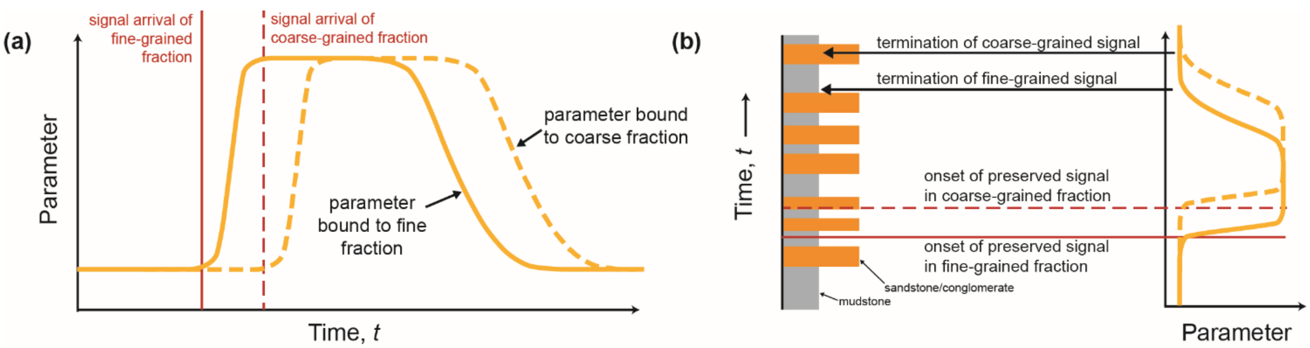


*Figure 6 Signal arrival times in the deposition area bound to different hydraulic grain size fractions in (a) representation of parameter expression versus time and (b) schematic expression in the stratigraphic record. This is one expression of many possible scenarios and is not meant to imply a general prediction (see text for discussion).*

## 5.2 Completeness of the stratigraphic record

Signals can be preserved in a wide variety of sedimentary sinks. Terrestrial archives that are frequently analyzed to decipher signals comprise alluvial fans (**Fig. 1**, Guerit et al., 2014, 2016; D'Arcy et al., 2017; Mason and Romans, 2018), lacustrine sediments (e.g., Dietze et al., 2014; Ramisch et al., 2018), and fluvial channels and floodplains (e.g., Foreman et al., 2012; Chen et al., 2018). In the shallow marine realm, signals can be stored in deltas (e.g., Jonell et al., 2017) and on the shelf (Ogston et al., 2000). The continental slope can host signal-preserving sediment archives within submarine canyons (Brocheray et al., 2014) and intraslope basins (Bernhardt et al., 2017). On the lower slope to basin floor, catchment signals are typically preserved in submarine channels (Jobe et al., 2015) and their levees (Dennielou et al., 2006; Toucanne et al., 2012; Bonneau et al., 2014; Hülscher et al., 2019), within lobes in submarine fans (Prélat and Hodgson, 2013; Spychala et al., 2017; Hessler and Fildani, 2019), basin-plain turbidites (Romans et al., 2009; Clare et al., 2015) or within hemipelagic sedimentation (Wheatcroft and Sommerfield, 2005). However, in most sinks, sediment deposition is not continuous, and phases of non-deposition, erosion or lateral channel movement result in stratigraphic gaps, or hiatuses. Hence, estimations of the completeness and fidelity of the stratigraphic record are required for signal inversion.

The fragmentary nature of stratigraphic records has been characterized by the catastrophic 'more gaps than record' paradigm (Ager, 1993) or as a 'set of frozen accidents' (Miall, 2015). A complete record is defined as one that does not encompass hiatuses longer than the time interval of successive sampling (Sadler, 1981; Kemp, 2012). Sadler (1981) proposed a simple means of estimating the expected stratigraphic completeness as a ratio of the local stratigraphic accumulation rate to a global average accumulation rate of similar depositional environments based on global regression analysis (note also the refined approach by Anders et al., 1987). Later, stochastic numerical models were developed to estimate stratigraphic completeness further stressing that the notion of stratigraphic completeness is meaningful only when scaled to the time scale of interest (Tipper, 1983; Strauss and Sadler, 1989; Kemp, 2012). Consequently, the maximal temporal resolution of a sedimentary archive is determined by the minimum time period at which a record is complete (Kemp and Sexton, 2014) and expected completeness tends to zero as the time scale of interest becomes shorter (Strauss and Sadler, 1989). However, in cases where the full three-dimensionality of the system can be assessed (e.g., Quaternary sediment budget analysis; Covault et al., 2011; Watkins et al., 2019), such measurement interval biases can be mitigated (Sadler and Jerolmack, 2015).

In addition, changes in hiatus duration and distribution can alter signal preservation. Kemp (2012) introduced the concept of stratigraphic fidelity, which is defined as the ability of a sediment archive to record the rate of geomorphic or geologic processes at the time scale of interest. Numerical experiments showed that a sediment archive can be complete with regard to the time scale of interest (e.g., signal cyclicity), but its stratigraphic fidelity can still be compromised due to the distribution of small-scale hiatuses (Kemp, 2012). Combining both of these concepts - completeness and fidelity -, stochastic modeling of synthetic records revealed spatiotemporally variable sedimentation and non-deposition can significantly influence the reconstructed *signal onset time*, duration and magnitude of sediment parameter changes (Trampush and Hajek, 2017).

A recent framework developed to estimate signal storage capacity of a certain environment has been put forward in a review by Straub et al. (2020) and references therein. Straub et al. (2020) quantify the *compensation time* ($T_c$) to predict signal-storage capacity of a SRS. The compensation time represents the maximum timescale of autogenic reorganization; that is patterns, variability, or dynamics as a consequence of interactions and feedbacks within the SRS as opposed to changes in boundary conditions. Basically, within a channelized SRS, $T_c$ is the time required to fill the channel with sediment (Sheets et al., 2002; Wang et al., 2011; Straub et al., 2020). Only after the channel is filled and $T_c$ has passed, sediment (and signals) will be deposited outside the confined channel and preserved in sedimentary archives outside channels (Sheets et al., 2002; Wang et al., 2011; Straub et al., 2020). Hence, the compensation timescale describes the minimum time before a signal gets incorporated in regional stratigraphy and is expressed as

$$T_c = \frac{l}{r} \quad \text{(eq. 8),}$$

with $l$ representing the autogenic vertical roughness scale of the surface of the depositional segment (e.g., maximum channel depth, where deep channels represent high surface roughness and vice versa) and $r$ denotes the long-term aggradation rate of the system (Sheets et al., 2002; Wang et al., 2011; Toby et al., 2019; Straub et al., 2020). The concept of $T_c$ is based on fluvial and deltaic sediment transport processes mostly in confined channels, with channel overtopping only during ephemeral flooding events (Sheets et al., 2002; Wang et al., 2011; Straub et al., 2020). Therefore, an exception to the application of $T_c$ might be submarine channel-levee systems on submarine fans- a common sink for terrestrial sediment – where sediment transport is dominated by debris flows and turbidity currents (Piper and Normark, 2001; Posamentier and Kolla, 2003). Superelevation of turbidity currents enables frequent sediment deposition on submarine levees even before the entire channel depth is filled with sediment (see section 4.2. for explanation). Hence, submarine levees can record signals below the characteristic $T_c$. While the frequency of turbidity currents determines the minimum time, the maximum time over which signals can be preserved in levee stratigraphy is given by the lifetime of a submarine channel (Dennielou et al., 2006; Toucanne et al., 2012; Bonneau et al., 2014). Lifetimes of submarine channel-levee systems vary from short-lived ones of several 100 years or less (Schwenk et al., 2003) to long-lived features of 6-8 million years (Bernhardt et al., 2012; Daniels et al., 2019; Hülscher et al., 2019). On a timescale larger than the channel's lifetime, the concept of $T_c$ (**eq. 8**) is again applicable in channel-levee systems and submarine fans.

The Lobyte3D stratigraphic forward model has been designed specifically to test for signal preservation in submarine fans and power spectrum analyses were used in the resulting strata to test for a 'signal bump' in the frequency spectrum (Burgess et al., 2019). First results indicate that the axial zone of the submarine fan has the highest probability of signal preservation (Burgess et al., 2019). However, other numerical modeling approaches of stratigraphy have been used to similarly test the likelihood of a stratigraphic section to preserve signals (Groenenberg et al., 2010; Harris et al., 2016; Hawie et al., 2018; Salles et al., 2018; Yuan et al., 2019b; Falivene et al., 2020).

# 6 Summary and future perspectives

## 6.1 Environmental signals

We have expanded the definition of environmental signals from changes in $Q_s$ to changes in any sedimentary parameter of interest (e.g., $Q_s$, grain size distribution, geochemical or isotopic composition and many more) related to a change in boundary conditions. Those signals are generated during transient landscape adjustment, and hence, are indicative of changes in boundary conditions. In order to preserve those signals, the signal-containing sediment needs to be transported along SRSs to a long-term sink (**Fig. 1**). Oftentimes, the parameter of interest is bound to a certain grain size fraction only. As sediment transport times highly vary with grain size, shape and density, we suggest investigating signal propagation by grouping signals in *hydraulic grain size fractions* that are transported jointly (**Fig. 2**). A *hydraulic grain size fraction* contains a size range of siliciclastic sediments (e.g., sand or silt) and their hydraulic equivalents. However, further investigation is required, in particular regarding the transport behavior of non-siliciclastic material and the according assignment to a certain *hydraulic grain size fraction*. Ideally, each transported grain can be assigned to a *hydraulic grain size fraction* with a certain probability based on a combination of quantifiable characteristics, e.g. material density, weight, degree of sphericity and others. Moreover, grain sizes reduce during transport due to abrasion and attrition, such that a single grain can move into a smaller *hydraulic grain size fraction* during transport. To date, a number of studies have quantified the rate of grain size reduction during transport (Sternberg, 1875; Kuenen, 1956; Bradley, 1970; Attal and Lavé, 2006, 2009; Dingle et al., 2017), but we still lack detailed knowledge about the role of grain composition on the rate of size reduction.

## 6.2 Times of signal generation and transfer

In order to reliably reconstruct past environmental conditions from parameter measurements (signals) in sedimentary archives, the time difference between the change in environmental boundary conditions and the signal arrival time in the archive — the *total signal lag time* — is essential (**Fig. 4**). The *total signal lag time* is the sum of the *signal onset time* (time between change in boundary conditions and onset of signal generation) and *signal transfer time* (time to transport the sediment carrying signal from the source to the sink). It is important to note that the *total signal lag time* is different from the *landscape response time*, which describes the duration of topographic landscape adjustment. Consequently, signals created due to short period climate changes can still be detectable in terrestrial and marine archives, even when transported in large river systems.

The *signal onset time* varies greatly with the parameter of interest and needs to be investigated for each parameter individually. *Signal transfer times* are mainly determined by the boundary conditions of SRSs. *Signal transfer times* will increase when grains are immobile within the active river channel or during long-term storage outside the active channel (**Fig. 5**). Both grain mobility and storage probability differ between *hydraulic grain size fractions*. Consequently, *signal transfer times* vary greatly between different parameters of interest and, therefore, need to be investigated for each *hydraulic grain size fraction* separately. To date, our knowledge on grain mobility especially on centennial, millennial and million-year time scales is still limited. Future research, in particular investigating the amplitude and frequency of river discharge or turbidity currents on the initiation of grain motion, will advance our understanding about the fraction of time a certain grain spends immobile on the channel bed versus in transport over these time scales. The storage probability outside the active channel is also affected by discharge amplitude and frequency, as both set the frequency of overbank flows. In addition, the storage probability is a function of vertical and lateral channel mobility, which in turn depends on climatic and tectonic boundary conditions. Further work investigating how prevailing tectonic and climatic boundary conditions are linked to rates of channel mobility will improve our understanding of sediment storage probability and times along SRSs.

In order to quantify the influence of individual factors on sediment transfer times, tools to measure sediment transport times are key. Although methods to quantify sediment transfer times have evolved, the precise measurement of the time sediment requires to move from the source to the sink is still a key challenge. Currently applied methods (**section 4.3**) are oftentimes limited to a certain grain size, mineralogy, or timescale. Developing methods that can, for example, be applied to the whole range of grain sizes will allow a direct comparison of grain size related transport times and hence uncover differences in signal transfer times. Similar to the multi-proxy approach used in paleoclimate reconstructions, successfully constraining sediment transfer times at the scale of SRSs will require integration of multiple methods targeting distinct fractions of the preserved sediment archive, which are interpreted and synthesized in a coordinated and interdisciplinary way. We also note that if these times are to be quantified and used to interpret system-scale behavior, methods that incorporate and propagate uncertainty that originates from the chronometric tool (e.g., error bars on determined ages) must be developed.

### 6.3 Signal preservation

In addition, reconstructions of past conditions from sedimentary signals not only require a detailed understanding of the duration of signal transfer along the SRSs, but also on the degree of signal modification and signal preservation in stratigraphy (time of signal arrival, stratigraphic completeness and fidelity). Signal modification has been attributed to autogenic fluctuations in sediment transport rates, transient sediment storage along SRSs, sediment abrasion during transport and, and signal dilution due to mixing with differently sourced sediments. In case signals make it to the sink, several signals generated by the same change in boundary conditions, but bound to different *hydraulic grain size fractions*, might differ in signal arrival times in the sink and, hence, might not be embedded in the same stratigraphic layer (**Fig. 6**). To date, studies investigating how a single event can be 'smeared' in the stratigraphic record due to *hydraulic grain size fraction* dependent differences in *signal arrival times* are rare. Further work is required, for example by comparing grain size-dependent compositional signatures between and among multiple SRS segments of a common age. Also, the degree of archive completeness and fidelity needs to be evaluated. Hiatuses in the record need to be shorter than the selected sampling interval (completeness), and the distribution of these hiatuses need to allow for reliable signal preservation (fidelity). In summary, a sedimentary signal may be best transferred in systems with high vertical roughness (deep channels/ high confinement) and low aggradation rates, ensuring minimal transient sediment storage. In contrast, a signal is best stored in systems with low vertical roughness and high accumulation rates, resulting in low *compensation timescales* (maximum timescale of autogenic reorganization and, hence, minimum time before a signal gets incorporated in regional stratigraphy).

### 6.4 Approach to holistic reconstructions of landscape response

Taken together, to holistically reconstruct landscape response to changes in boundary conditions, we strongly recommend combining sediment parameters from different *hydraulic grain size fractions*. For each parameter of interest, the goal should be to be able to answer the following five questions:

(1) Which *hydraulic grain size fraction* is the parameter of interest bound to?

(2) What is the *time of signal arrival* in the sink?

(3) What is the *signal transfer time* (depending on *hydraulic grain size fraction*, catchment geometries and tectonic and climatic boundary conditions) for the parameter of interest?

(4) What is the *signal onset time* for the parameter of interest?

(5) Which signals can confidently be recorded in the chosen sedimentary archive (completeness and fidelity)? How does the estimated *compensation timescale* for the SRS compare to the hypothesized *signal duration time* (see exception for submarine channel-levee systems)?

Depending on how question 1 to 5 are answered, the chosen sedimentary archive and parameter of interest allows for the reconstruction of the time and/or duration of changes in tectonic or climatic boundary conditions or not. We further recommend using stochastic or stratigraphic forward models appropriate to the specific research question to generate testable hypotheses and/ or to perform sensitivity analyses of the stratigraphic archive of choice to a specific signal.

Ideally, highly accurate reconstructions of past environmental conditions require that all the above — times of signal transfer, degree of signal modification, and completeness and fidelity of signal storage — can be quantified and separated from one another. Thus, to advance in the field of environmental reconstructions, efforts should continue to quantify any of these processes in isolation.

## 7 Notation

| | | |
|---|---|---|
| $D$ | grain diameter | m |
| $g$ | acceleration due to gravity (= 9.807) | m $s^{-2}$ |
| $h$ | flow depth | m |
| $K$ | diffusivity coefficient | $m^2$ $s^{-1}$ |
| $L$ | river segment length | m |
| $Q_s$ | sediment discharge | $m^3$ $s^{-1}$ or kg $s^{-1}$ |
| $Q_w$ | water discharge | $m^3$ $s^{-1}$ |
| $S$ | channel gradient | - |
| $t$ | time | s |
| $T_{eq}$ | river response time | s |
| $u$ | turbidity current velocity | m $s^{-1}$ |
| $z$ | elevation | m |
| $\kappa$ | eddy viscosity | Pa s = N s $m^{-2}$ |
| $\mu$ | dynamic viscosity | Pa s = N s $m^{-2}$ |
| $\rho_s$ | sediment or grain density (material dependent) | kg $m^{-3}$ |
| $\rho_w$ | water density (=1000) | kg $m^{-3}$ |
| $\tau$ | shear stress | Pa = N $m^{-2}$ |
| $\tau*$ or $\theta$ | Shield's parameter or Shield's criterion = non-dimensional shear stress | - |
| $\tau_b$ | bed shear stress; stress exerted by the fluid on the channel bed | Pa = N $m^{-2}$ |
| $\tau_b*$ | non-dimensional bed shear stress | - |
| $\tau_c$ | critical shear stress for initiation of grain motion | Pa = N $m^{-2}$ |
| $\tau_c*$ | non-dimension critical shear stress | - |

## 8 Glossary

**Adjustment time** — Equivalent to landscape response time

**Analytical response time** — Theory-based (diffusion or advection) river response times, which describe the time of the river longitudinal profile to attain new steady state (after Densmore et al., 2007b; Allen, 2008b).

**Compensation timescale** — Maximum timescale of autogenic reorganization in a SRS and, hence, minimum time before a signal gets incorporated in regional stratigraphy.

**e-folding response time** — Timescale related to an exponential function: One e-folding time is equivalent to the time when the parameter of interest has decreased to 37% (≈1/e) or increased by the factor of *e* relative to its initial value.

**Environmental signal** — Change in any sedimentary parameter of interest through time that can be linked to a change in boundary condition.

**Hydraulic grain size fraction** — A size range of siliciclastic sediments and material that is transported jointly, i.e. the hydraulic equivalents.

| | |
|---|---|
| **Intrinsic equilibrium time** | The river response time for a 1D fluvial system described by a diffusion equation (after Paola et al., 1992). |
| **Landscape response time** | Duration of topographic landscape adjustment after a change in boundary conditions. |
| **Reaction time** | Time lag between the onset of change in boundary conditions and the first topographic adjustment (after Bull, 1991). |
| **Relaxation time** | Time period between the first topographic adjustment and the achievement of new steady state (after Bull, 1991). |
| | Response times measured by fitting an exponential curve to a parameter time-series (after Densmore et al., 2007b; Allen, 2008b). |
| **River response time** | Duration of river longitudinal profile adjustment after a change in boundary conditions. |
| **Sediment transport time** | Duration of sediment transport along SRSs. |
| **Signal arrival time** | Moment of first detectable parameter change in the sink. |
| **Signal duration time** | Time of a measurable change in parameter of interest in the source region. |
| **Signal onset time** | Time until a measurable change in parameter of interest in the source region is generated. |
| **Signal transfer time** | Time required for the signal to travel to the deposition zone. |
| **Total signal lag time** | Time between change in boundary conditions and onset of measurable change in parameter of interest in the deposition zone. |

## 9 Conflict of Interest

The authors declare that the research was conducted in the absence of any commercial or financial relationships that could be construed as a potential conflict of interest.

## 10 Author Contributions

S.T. and A.B. designed the review study. S.T. and A.B. led the writing of the manuscript with contributions from all authors.

## 11 Funding

## 12 Acknowledgments

We thank Jens M. Turowski and Andrew D. Wickert, who commented on an earlier version of this manuscript.

## 13 References

Ager, D. V. (1993). *The nature of the stratigraphical record*.

Allen, J. R. L. (1974). Reaction, relaxation and lag in natural sedimentary systems: general principles, examples and lessons. *Earth-Science Rev.* 10, 263–342.

Allen, P. A. (2008a). From landscapes into geological history. *Nature* 451, 274–276. doi:10.1038/nature06586.

Allen, P. A. (2008b). Time scales of tectonic landscapes and their sediment routing systems. *Geol. Soc. London, Spec. Publ.*, 7–28.

Allen, P. A. (2017). *Sediment routing systems: The fate of sediment from source to sink*. Cambridge University Press.

Allen, P. A., Armitage, J. J., Allen, P. A., Armitage, J. J., Whittaker, A. C., Michael, N. A., et al. (2015). Fragmentation Model of the Grain Size Mix of Sediment Supplied to Basins Fragmentation Model of the Grain Size Mix of Sediment Supplied to Basins. doi:10.1086/683113.

Allen, P. A., Armitage, J. J., Carter, A., Duller, R. A., and Whittaker, A. C. (2013). The Qs problem: Sediment volumetric balance of proximal foreland basin systems. *Sedimentology* 60, 102–130. doi:10.1111/sed.12015.

Allen, P. A., and Densmore, A. L. (2000). Sediment flux from an uplifting fault block. *Basin Res.* 12, 367–380. doi:10.1111/j.1365-2117.2000.00135.x.

Anders, M. H., Krueger, S. W., and Sadler, P. M. (1987). A new look at sedimentation rates and the completeness of the stratigraphic record. *J. Geol.* 95, 1–14.

Anderson, J. B. J. B., Kurtz, D. D. D., Domack, E. W. W., and Balshaw, K. M. M. (1980). Glacial and glacial marine sediments of the Antarctic continental shelf. *J. Geol.* 88, 399–414.

Armitage, J. J., Burgess, P. M., Hampson, G. J., and Allen, P. A. (2018a). Deciphering the origin of cyclical gravel front and shoreline progradation and retrogradation in the stratigraphic record. *Basin Res.* 30, 15–35.

Armitage, J. J., Duller, R. A., Whittaker, A. C., and Allen, P. A. (2011). Transformation of tectonic and climatic signals from source to sedimentary archive. *Nat. Geosci.* 4, 231–235. doi:10.1038/ngeo1087.

Armitage, J. J., Dunkley Jones, T., Duller, R. A., Whittaker, A. C., and Allen, P. A. (2013). Temporal buffering of climate-driven sediment flux cycles by transient catchment response. *Earth Planet.*

*Sci. Lett.* 369–370, 200–210. doi:10.1016/j.epsl.2013.03.020.

Armitage, J. J., Whittaker, A. C., Zakari, M., and Campforts, B. (2018b). Numerical modelling landscape and sediment flux response to precipitation rate change. *Earth Surf. Dyn.* 6, 77–99. doi:10.5194/esurf-2017-34.

Attal, M., and Lavé, J. (2006). Changes of bedload characteristics along the Marsyandi River (central Nepal): Implications for understanding hillslope sediment supply, sediment load evolution along fluvial networks, and denudation in active orogenic belts. *Tectonics, Clim. Landsc. Evol.* 398, 143–171. doi:10.1130/2006.2398(09).

Attal, M., and Lavé, J. (2009). Pebble abrasion during fluvial transport: Experimental results and implications for the evolution of the sediment load along rivers. *J. Geophys. Res. Earth Surf.* 114. doi:10.1029/2009JF001328.

Azpiroz-Zabala, M., Cartigny, M. J. B., Talling, P. J., Parsons, D. R., Sumner, E. J., Clare, M. A., et al. (2017). Newly recognized turbidity current structure can explain prolonged flushing of submarine canyons. *Sci. Adv.* 3, e1700200.

Baby, G., Guillocheau, F., Braun, J., Robin, C., and Dall'Asta, M. (2020). Solid sedimentation rates history of the Southern African continental margins: Implications for the uplift history of the South African Plateau. *Terra Nov.* 32, 53–65.

Balco, G., and Stone, J. O. H. (2005). Measuring middle Pleistocene erosion rates with cosmic-ray-produced nuclides in buried alluvial sediment, Fisher Valley, southeastern Utah. *Earth Surf. Process. Landforms* 30, 1051–1067. doi:10.1002/esp.1262.

Bataille, C. P., Ridgway, K. D., Colliver, L., and Liu, X.-M. (2019). Early Paleogene fluvial regime shift in response to global warming: A subtropical record from the Tornillo Basin, west Texas, USA. *Bulletin* 131, 299–317.

Baynes, E. R. C., Lague, D., Attal, M., Gangloff, A., Kirstein, L. A., and Dugmore, A. J. (2018). River self-organisation inhibits discharge control on waterfall migration. *Sci. Rep.* 8, 1–8.

Bernhardt, A., Hebbeln, D., Regenberg, M., Lückge, A., and Strecker, M. R. (2016). Shelfal sediment transport by an undercurrent forces turbidity-current activity during high sea level along the Chile continental margin. *Geology* 44, 295–298.

Bernhardt, A., Jobe, Z. R., Grove, M., and Lowe, D. R. (2012). Palaeogeography and diachronous infill of an ancient deep-marine foreland basin, Upper Cretaceous Cerro Toro Formation, Magallanes Basin. *Basin Res.* 24, 269–294.

Bernhardt, A., Melnick, D., Jara-Muñoz, J., Argandoña, B., González, J., and Strecker, M. R. (2015). Controls on submarine canyon activity during sea-level highstands: The Biobío canyon system offshore Chile. *Geosphere* 11, 1226–1255.

Bernhardt, A., Schwanghart, W., Hebbeln, D., Stuut, J.-B. W., and Strecker, M. R. (2017). Immediate propagation of deglacial environmental change to deep-marine turbidite systems along the Chile convergent margin. *Earth Planet. Sci. Lett.* 473, 190–204.

Blom, A., Chavarrías, V., Ferguson, R. I., and Viparelli, E. (2017). Advance, Retreat, and Halt of Abrupt Gravel-Sand Transitions in Alluvial Rivers. *Geophys. Res. Lett.* 44, 9751–9760. doi:10.1002/2017GL074231.

Blöthe, J. H., and Korup, O. (2013). Millennial lag times in the Himalayan sediment routing system. *Earth Planet. Sci. Lett.* 382, 38–46. doi:10.1016/j.epsl.2013.08.044.

Blum, M. D., and Törnqvist, T. E. (2000). Fluvial responses to climate and sea-level change: a review and look forward. *Sedimentology* 47, 2–48.

Blum, M., Rogers, K., Gleason, J., Najman, Y., Cruz, J., and Fox, L. (2018). Allogenic and Autogenic Signals in the Stratigraphic Record of the Deep-Sea Bengal Fan. *Sci. Rep.* 8. doi:10.1038/s41598-018-25819-5.

Bonneau, L., Jorry, S. J., Toucanne, S., Silva Jacinto, R., and Emmanuel, L. (2014). Millennial-scale response of a western Mediterranean river to late Quaternary climate changes: a view from the deep sea. *J. Geol.* 122, 687–703.

Bonnet, S., and Crave, A. (2003). Landscape response to climate change: Insights from experimental modeling and implications for tectonic versus climatic uplift of topography. *Geology* 31, 123–126.

Bracken, L. J., Turnbull, L., Wainwright, J., and Bogaart, P. (2015). Sediment connectivity: a framework for understanding sediment transfer at multiple scales. *Earth Surf. Process. Landforms* 40, 177–188.

Bradley, D. N., and Tucker, G. E. (2013). The storage time, age, and erosion hazard of laterally accreted sediment on the floodplain of a simulated meandering river. *J. Geophys. Res. Earth Surf.* 118, 1308–1319.

Bradley, N. D., and Tucker, G. E. (2012). Measuring gravel transport and dispersion in a mountain river using passive radio tracers. *Earth Surf. Process. Landforms* 37, 1034–1045.

Bradley, W. C. (1970). Effect of Weathering on Abrasion of Granitic Gravel, Colorado River (Texas). *Geol. Soc. Am. Bull.* 81, 61–80.

Braun, J., Voisin, C., Gourlan, A. T., and Chauvel, C. (2015). Erosional response of an actively uplifting mountain belt to cyclic rainfall variations. *Earth Surf. Dyn.* 3, 1–14. doi:10.5194/esurf-3-1-2015.

Brocheray, S., Cremer, M., Zaragosi, S., Schmidt, S., Eynaud, F., Rossignol, L., et al. (2014). 2000 years of frequent turbidite activity in the Capbreton Canyon (Bay of Biscay). *Mar. Geol.* 347, 136–152.

Bufe, A., Turowski, J. M., Burbank, D. W., Paola, C., Wickert, A. D., and Tofelde, S. (2019). Controls on the lateral channel-migration rate of braided channel systems in coarse non-cohesive sediment. *Earth Surf. Process. Landforms* 44, 2823–2836. doi:10.1002/esp.4710.

Buffington, J. M., and Montgomery, D. R. (1997). A systematic analysis of eight decades of incipient motion studies , with special reference to gravel-bedded rivers g DS0. 33, 1993–2029.

Bull, W. B. (1991). *Geomorphic responses to climatic change*.

Burgess, P. M., and Hovius, N. (1998). Rates of delta progradation during highstands: consequences for timing of deposition in deep-marine systems. *J. Geol. Soc. London.* 155, 217–222.

Burgess, P. M., Masiero, I., Toby, S. C., and Duller, R. A. (2019). A big fan of signals? Exploring autogenic and allogenic process and product in a numerical stratigraphic forward model of submarine-fan development. *J. Sediment. Res.* 89, 1–12.

Caracciolo, L. (2020). Sediment generation and sediment routing systems from a quantitative provenance analysis perspective: Review, application and future development. *Earth-Science Rev.*, 103226. doi:10.1016/j.earscirev.2020.103226.

Carretier, S., Guerit, L., Harries, R., Regard, V., Maffre, P., and Bonnet, S. (2020). The distribution of sediment residence times at the foot of mountains and its implications for proxies recorded in sedimentary basins. *Earth Planet. Sci. Lett.* 546, 116448. doi:10.1016/j.epsl.2020.116448.

Carretier, S., Martinod, P., Reich, M., and Godderis, Y. (2016). Modelling sediment clasts transport during landscape evolution. *Earth Surf. Dyn.* 4, 237–251. doi:10.5194/esurf-4-237-2016.

Carretier, S., and Regard, V. (2011). Is it possible to quantify pebble abrasion and velocity in rivers using terrestrial cosmogenic nuclides? *J. Geophys. Res. Earth Surf.* 116.

Carretier, S., Regard, V., Leanni, L., and Farías, M. (2019). Long-term dispersion of river gravel in a canyon in the Atacama Desert, Central Andes, deduced from their 10Be concentrations. *Sci. Rep.* 9, 1–12. doi:10.1038/s41598-019-53806-x.

Carretier, S., Regard, V., Vassallo, R., Aguilar, G., Martinod, J., Riquelme, R., et al. (2015). Differences in 10 Be concentrations between river sand, gravel and pebbles along the western side of the central Andes. *Quat. Geochronol.* 27, 33–51. doi:10.1016/j.quageo.2014.12.002.

Carvajal, C. R., and Steel, R. J. (2006). Thick turbidite successions from supply-dominated shelves during sea-level highstand. *Geology* 34, 665–668.

Castelltort, S., and Van Den Driessche, J. (2003). How plausible are high-frequency sediment supply-driven cycles in the stratigraphic record? *Sediment. Geol.* 157, 3–13. doi:10.1016/S0037-0738(03)00066-6.

Chabaux, F., Blaes, E., Granet, M., di Chiara Roupert, R., and Stille, P. (2012). Determination of transfer time for sediments in alluvial plains using 238U-234U-230Th disequilibria: the case of the Ganges river system. *Comptes Rendus Geosci.* 344, 688–703.

Chabaux, F., Granet, M., Pelt, E., France-Lanord, C., and Galy, V. (2006). 238U–234U–230Th disequilibria and timescale of sedimentary transfers in rivers: clues from the Gangetic plain rivers. *J. Geochemical Explor.* 88, 373–375.

Charreau, J., Blard, P. H., Puchol, N., Avouac, J. P., Lallier-Vergès, E., Bourlès, D., et al. (2011). Paleo-erosion rates in Central Asia since 9Ma: A transient increase at the onset of Quaternary glaciations? *Earth Planet. Sci. Lett.* 304, 85–92. doi:10.1016/j.epsl.2011.01.018.

Chen, C., Guerit, L., Foreman, B. Z., Hassenruck-Gudipati, H. J., Adatte, T., Honegger, L., et al. (2018). Estimating regional flood discharge during Palaeocene-Eocene global warming. *Sci. Rep.* 8, 1–8.

Clare, M. A., Talling, P. J., and Hunt, J. E. (2015). Implications of reduced turbidity current and landslide activity for the Initial Eocene Thermal Maximum–evidence from two distal, deep-water sites. *Earth Planet. Sci. Lett.* 420, 102–115.

Clarke, L., Quine, T. A., and Nicholas, A. (2010). An experimental investigation of autogenic behaviour during alluvial fan evolution. *Geomorphology* 115, 278–285. doi:10.1016/j.geomorph.2009.06.033.

Clift, P. D., and Giosan, L. (2014). Sediment fluxes and buffering in the post-glacial Indus Basin. *Basin Res.* 26, 369–386.

Clift, P. D., Giosan, L., Blusztajn, J., Campbell, I. H., Allen, C., Pringle, M., et al. (2008). Holocene erosion of the Lesser Himalaya triggered by intensified summer monsoon. *Geology* 36, 79–82.

Cossu, R., and Wells, M. G. (2012). A comparison of the shear stress distribution in the bottom boundary layer of experimental density and turbidity currents. *Eur. J. Mech.* 32, 70–79.

Coulthard, T. J., and Van De Wiel, M. J. (2007). Quantifying fluvial non linearity and finding self organized criticality? Insights from simulations of river basin evolution. *Geomorphology* 91, 216–235. doi:10.1016/j.geomorph.2007.04.011.

Coulthard, T. J., and Van De Wiel, M. J. (2013). Climate, tectonics or morphology: what signals can we see in drainage basin sediment yields ? *Earth Surf. Dyn.* 1, 13–27. doi:10.5194/esurf-1-13-2013.

Covault, J. A., and Graham, S. A. (2010). Submarine fans at all sea-level stands: Tectono-morphologic and climatic controls on terrigenous sediment delivery to the deep sea. *Geology* 38, 939–942.

Covault, J. A., Romans, B. W., Fildani, A., Mcgann, M., and Graham, S. A. (2010). Rapid Climatic Signal Propagation from Source to Sink in a Southern California Sediment-Routing System. *J. Geol.* 118, 247–259. doi:10.1086/651539.

Covault, J. A., Romans, B. W., Graham, S. A., Fildani, A., and Hilley, G. E. (2011). Terrestrial source to deep-sea sink sediment budgets at high and low sea levels: Insights from tectonically active Southern California. *Geology* 39, 619–622. doi:10.1130/G31801.1.

Curran, J. C., and Wilcock, P. R. (2005). Effect of sand supply on transport rates in a gravel-bed channel. *J. Hydraul. Eng.* 131, 961–967.

D’Arcy, M., Roda-Boluda, D. C., and Whittaker, A. C. (2017). Glacial-interglacial climate changes recorded by debris flow fan deposits, Owens Valley, California. *Quat. Sci. Rev.* 169, 288–311. doi:10.1016/j.quascirev.2017.06.002.

D’Arcy, M., Roda Boluda, D. C., Whittaker, A. C., and Carpineti, A. (2015). Dating alluvial fan surfaces in Owens Valley, California, using weathering fractures in boulders. *Earth Surf. Process. Landforms* 40, 487–501. doi:10.1002/esp.3649.

D'Arcy, M., Whittaker, A. C., and Roda-Boluda, D. C. (2016). Measuring alluvial fan sensitivity to past climate changes using a self-similarity approach to grain-size fining, Death Valley, California. *Sedimentology* 64.2, 388–424. doi:10.1111/sed.12308.

D'Orsay, A. M., and Van De Poll, H. W. (1985). Quartz-grain surface textures: Evidence for middle Carboniferous glacial sediment input to the Parrsboro Formation of Nova Scotia. *Geology* 13, 285–287. doi:10.1130/0091-7613(1985)13<285:QSTEFM>2.0.CO;2.

Da Silva, A. C., De Vleeschouwer, D., Boulvain, F., Claeys, P., Fagel, N., Humblet, M., et al. (2013). Magnetic susceptibility as a high-resolution correlation tool and as a climatic proxy in Paleozoic rocks – Merits and pitfalls: Examples from the Devonian in Belgium. *Mar. Pet. Geol.* 46, 173–189. doi:https://doi.org/10.1016/j.marpetgeo.2013.06.012.

Daniels, B. G., Hubbard, S. M., Romans, B. W., Malkowski, M. A., Matthews, W. A., Bernhardt, A., et al. (2019). Revised chronostratigraphic framework for the Cretaceous Magallanes-Austral Basin, Última Esperanza Province, Chile. *J. South Am. Earth Sci.* 94, 102209.

Davy, P., and Crave, A. (2000). Upscaling local-scale transport processes in large-scale relief dynamics. *Phys. Chem. Earth, Part A Solid Earth Geod.* 25, 533–541.

Davy, P., and Lague, D. (2009). Fluvial erosion/transport equation of landscape evolution models revisited. *J. Geophys. Res. Earth Surf.* 114.

Dennielou, B., Huchon, A., Beaudouin, C., and Berné, S. (2006). Vertical grain-size variability within a turbidite levee: Autocyclicity or allocyclicity? A case study from the Rhône neofan, Gulf of Lions, Western Mediterranean. *Mar. Geol.* 234, 191–213.

Densmore, A. L., Allen, P. A., and Simpson, G. (2007a). Development and response of a coupled catchment fan system under changing tectonic and climatic forcing. *J. Geophys. Res. Earth Surf.* 112, 1–16. doi:10.1029/2006JF000474.

Densmore, A. L., Gupta, S., Allen, P. A., and Dawers, N. H. (2007b). Transient landscapes at fault tips. *J. Geophys. Res. Earth Surf.* 112, 1–16. doi:10.1029/2006JF000560.

DePaolo, D. J. (2012). *Neodymium isotope geochemistry: an introduction*. Springer Science & Business Media.

DePaolo, D. J., Maher, K., Christensen, J. N., and McManus, J. (2006). Sediment transport time measured with U-series isotopes: results from ODP North Atlantic drift site 984. *Earth Planet. Sci. Lett.* 248, 394–410.

DiBiase, R. A., and Lamb, M. P. (2013). Vegetation and wildfire controls on sediment yield in bedrock landscapes. *Geophys. Res. Lett.* 40, 1093–1097.

Diefendorf, A. F., and Freimuth, E. J. (2017). Extracting the most from terrestrial plant-derived n-alkyl lipids and their carbon isotopes from the sedimentary record: A review. *Org. Geochem.* 103, 1–21. doi:10.1016/j.orggeochem.2016.10.016.

Dietrich, W. E. (1982). Settling velocity of natural particles. *Water Resour. Res.* 18, 1615–1626. doi:10.1029/WR018i006p01615.

Dietze, E., Maussion, F., Ahlborn, M., Diekmann, B., Hartmann, K., Henkel, K., et al. (2014). Sediment transport processes across the Tibetan Plateau inferred from robust grain-size end members in lake sediments. *Clim. Past* 10, 91–106.

Dingle, E. H., Attal, M., and Sinclair, H. D. (2017). Abrasion-set limits on Himalayan gravel flux. *Nature* 544, 471–474. doi:10.1038/nature22039.

Dingle, E. H., Sinclair, H. D., Venditti, J. G., Attal, M., Kinnaird, T. C., Creed, M., et al. (2020). Sediment dynamics across gravel-sand transitions: Implications for river stability and floodplain recycling. XX, 1–5. doi:10.1130/G46909.1/4944757/g46909.pdf.

Dommain, R., Andama, M., McDonough, M. M., Prado, N. A., Goldhammer, T., Potts, R., et al. (2019). The Challenges of Reconstructing Tropical Biodiversity With Sedimentary Ancient DNA. *Front. Ecol. Evol.* 8. Available at: https://publishup.uni-potsdam.de/frontdoor/index/index/docId/47429.

Dosseto, A., Bourdon, B., Gaillardet, J., Maurice-Bourgoin, L., and Allegre, C. J. (2006). Weathering and transport of sediments in the Bolivian Andes: Time constraints from uranium-series isotopes. *Earth Planet. Sci. Lett.* 248, 759–771.

Du, J. Z., Zhang, J., and Baskaran, M. (2012). "Applications of short-lived radionuclides (7Be, 210Pb, 210Po, 137Cs and 234Th) to trace the sources, transport pathways and deposition of particles/sediments in rivers, estuaries and coasts," in *Handbook of environmental isotope geochemistry* (Springer), 305–329.

Dubille, M., and Lavé, J. (2015). Rapid grain size coarsening at sandstone/conglomerate transition: similar expression in Himalayan modern rivers and Pliocene molasse deposits. *Basin Res.* 27, 26–42. doi:10.1111/bre.12071.

Ducassou, E., Mulder, T., Migeon, S., Gonthier, E., Murat, A., Revel, M., et al. (2008). Nile floods recorded in deep Mediterranean sediments. *Quat. Res.* 70, 382–391.

Duller, R. A., Armitage, J. J., Manners, H. R., Grimes, S. T., Jones, T. D., and Dunkley Jones, T. (2019). Delayed sedimentary response to abrupt climate change at the Paleocene-Eocene boundary, northern Spain. *Geology* 47, 159–162. doi:10.1130/G45631.1.

Duller, R. A., Whittaker, A. C., Fedele, J. J., Whitchurch, A. L., Springett, J., Smithells, R., et al. (2010). From grain size to tectonics. *J. Geophys. Res. Earth Surf.* 115, 1–19. doi:10.1029/2009JF001495.

Einstein, A. (1926). The cause of the formation of meanders in the courses of rivers and of the so-called Baer's law. *Naturwissenschaften* 14, 223–224.

Falivene, O., Prather, B. E., and Martin, J. (2020). Quantifying sand delivery to deep water during changing sea-level: Numerical models from the Quaternary Brazos Icehouse continental margin. *Basin Res.*

Fildani, A., Hessler, A. M., Mason, C. C., McKay, M. P., and Stockli, D. F. (2018). Late Pleistocene glacial transitions in North America altered major river drainages, as revealed by deep-sea sediment. *Sci. Rep.* 8, 1–8.

Fildani, A., Normark, W. R., Kostic, S., and Parker, G. (2006). Channel formation by flow stripping: Large-scale scour features along the Monterey East Channel and their relation to sediment waves. *Sedimentology* 53, 1265–1287.

Foreman, B. Z. (2014). Climate-driven generation of a fluvial sheet sand body at the Paleocene-Eocene boundary in north-west Wyoming (USA). *Basin Res.* 26, 225–241. doi:10.1111/bre.12027.

Foreman, B. Z., Heller, P. L., and Clementz, M. T. (2012). Fluvial response to abrupt global warming at the Palaeocene/Eocene boundary. *Nature* 491, 92–95. doi:10.1038/nature11513.

Forzoni, A., Storms, J. E. A., Whittaker, A. C., and de Jager, G. (2014). Delayed delivery from the sediment factory: Modeling the impact of catchment response time to tectonics on sediment flux and fluvio-deltaic stratigraphy. *Earth Surf. Process. Landforms* 39, 689–704. doi:10.1002/esp.3538.

Fryirs, K. (2013). (Dis) Connectivity in catchment sediment cascades: a fresh look at the sediment delivery problem. *Earth Surf. Process. Landforms* 38, 30–46.

Fülöp, R., Codilean, A. T., Wilcken, K. M., Cohen, T. J., Fink, D., Smith, A. M., et al. (2020). Million-year lag times in a post-orogenic sediment conveyor.

Galy, V., and Eglinton, T. (2011). Protracted storage of biospheric carbon in the Ganges-Brahmaputra basin. *Nat. Geosci.* 4, 843–847. doi:10.1038/ngeo1293.

Galy, V., France-Lanord, C., and Lartiges, B. (2008). Loading and fate of particulate organic carbon from the Himalaya to the Ganga-Brahmaputra delta. *Geochim. Cosmochim. Acta* 72, 1767–1787. doi:10.1016/j.gca.2008.01.027.

Ganti, V., Lamb, M. P., and McElroy, B. (2014). Quantitative bounds on morphodynamics and implications for reading the sedimentary record. *Nat. Commun.* 5. doi:10.1038/ncomms4298.

Garcin, Y., Schildgen, T. F., Torres Acosta, V., Melnick, D., Guillemoteau, J., Willenbring, J., et al. (2017). Short-lived increase in erosion during the African Humid Period: Evidence from the northern Kenya Rift. *Earth Planet. Sci. Lett.* 459, 58–69. doi:10.1016/j.epsl.2016.11.017.

Garcin, Y., Schwab, V. F., Gleixner, G., Kahmen, A., Todou, G., Séné, O., et al. (2012). Hydrogen isotope ratios of lacustrine sedimentary n-alkanes as proxies of tropical African hydrology: Insights from a calibration transect across Cameroon. *Geochim. Cosmochim. Acta* 79, 106–126. doi:10.1016/j.gca.2011.11.039.

Godard, V., Tucker, G. E., Burch Fisher, G., Burbank, D. W., and Bookhagen, B. (2013). Frequency-dependent landscape response to climatic forcing. *Geophys. Res. Lett.* 40, 859–863. doi:10.1002/grl.50253.

Goodbred, S., and Kuehl, S. A. (2000). Enormous Ganges-Brahmaputra sediment dischange during strengthened early Holocene monsoon. *Geology* 28, 1083–1086. doi:10.1130/0091-7613(2000)28<1083:EGSDDS>2.0.CO;2.

Goodbred, S. L. (2003). Response of the Ganges dispersal system to climate change: A source-to-sink view since the last interstade. *Sediment. Geol.* 162, 83–104. doi:10.1016/S0037-0738(03)00217-

3.

Goren, L., Willett, S. D., Herman, F., and Braun, J. (2014). Coupled numerical–analytical approach to landscape evolution modeling. *Earth Surf. Process. Landforms* 39, 522–545.

Gray, H. J., Tucker, G. E., Mahan, S. A., McGuire, C., and Rhodes, E. J. (2017). On extracting sediment transport information from measurements of luminescence in river sediment. *J. Geophys. Res. Earth Surf.* 122, 654–677.

Grimaud, J. L., Paola, C., and Voller, V. (2016). Experimental migration of knickpoints: Influence of style of base-level fall and bed lithology. *Earth Surf. Dyn.* 4, 11–23. doi:10.5194/esurf-4-11-2016.

Groenenberg, R. M., Hodgson, D. M., Prelat, A., Luthi, S. M., and Flint, S. S. (2010). Flow–deposit interaction in submarine lobes: Insights from outcrop observations and realizations of a process-based numerical model. *J. Sediment. Res.* 80, 252–267.

Guerit, L., Barrier, L., Jolivet, M., Fu, B., and Métivier, F. (2016). Denudation intensity and control in the Chinese Tian Shan: new constraints from mass balance on catchment-alluvial fan systems. *Earth Surf. Process. Landforms* 41, 1088–1106.

Guerit, L., Foreman, B. Z., Chen, C., Paola, C., and Castelltort, S. (2020). Autogenic delta progradation during sea-level rise within incised valleys. *Geology*.

Guerit, L., Métivier, F., Devauchelle, O., Lajeunesse, E., and Barrier, L. (2014). Laboratory alluvial fans in one dimension. *Phys. Rev. E* 90, 22203.

Guerit, L., Yuan, X.-P., Carretier, S., Bonnet, S., Rohais, S., Braun, J., et al. (2019). Fluvial landscape evolution controlled by the sediment deposition coefficient: Estimation from experimental and natural landscapes. *Geology* 47, 853–856. doi:10.1130/g46356.1.

Guillocheau, F., Rouby, D., Robin, C., Helm, C., Rolland, N., De Veslud, C. L. C., et al. (2012). Quantification and causes of the terrigeneous sediment budget at the scale of a continental margin: a new method applied to the Namibia–South Africa margin. *Basin Res.* 24, 3–30. doi:10.1111/j.1365-2117.2011.00511.x.

Hack, J. T. (1960). *Interpretation of erosional topography in humid temperate regions*. Bobbs-Merrill.

Hajek, E. A., and Straub, K. M. (2017). Autogenic sedimentation in clastic stratigraphy. *Annu. Rev. Earth Planet. Sci.* 45, 681–709.

Harris, A. D., Covault, J. A., Madof, A. S., Sun, T., Sylvester, Z., and Granjeon, D. (2016). Three-dimensional numerical modeling of eustatic control on continental-margin sand distributionA. d. harris et al. numerical modeling of eustatic control on continental-margin sand distribution. *J. Sediment. Res.* 86, 1434–1443.

Hawie, N., Covault, J. A., Dunlap, D., and Sylvester, Z. (2018). Slope-fan depositional architecture from high-resolution forward stratigraphic models. *Mar. Pet. Geol.* 91, 576–585.

Haynes, H., and Pender, G. (2007). Stress history effects on graded bed stability. *J. Hydraul. Eng.* 133, 343–349.

Heberer, B., Behrmann, J. H., and Rahn, M. K. (2011). Source-to-sink relationships along the South-Central Chilean margin: evidence from detrital apatite fission-track analysis. *Basin Res.* 23, 551–570.

Heerema, C. J., Talling, P. J., Cartigny, M. J., Paull, C. K., Bailey, L., Simmons, S. M., et al. (2020). What determines the downstream evolution of turbidity currents? *Earth Planet. Sci. Lett.* 532, 116023.

Helland, P. E., Huang, P.-H., and Diffendal, R. F. (1997). SEM Analysis of Quartz Sand Grain Surface Textures Indicates Alluvial/Colluvial Origin of the Quaternary "Glacial" Boulder Clays at Huangshan (Yellow Mountain), East-Central China. *Quat. Res.* 48, 177–186. doi:https://doi.org/10.1006/qres.1997.1916.

Hessler, A. M., and Fildani, A. (2019). Deep-sea fans: tapping into Earth's changing landscapes. *J. Sediment. Res.* 89, 1171–1179. doi:10.2110/jsr.2019.64.

Hickin, E. J., and Nanson, G. C. (1984). Lateral migration rates of river bends. *J. Hydraul. Eng.* 110, 1557–1567.

Hilley, G. E., and Strecker, M. R. (2005). Processes of oscillatory basin filling and excavation in a tectonically active orogen: Quebrada del Toro Basin, NW Argentina. *Bull. Geol. Soc. Am.* 117, 887–901. doi:10.1130/B25602.1.

Hinderer, M. (2012). From gullies to mountain belts: a review of sediment budgets at various scales. *Sediment. Geol.* 280, 21–59. doi:10.1016/j.sedgeo.2012.03.009.

Hjulstrom, F. (1955). Transportation of detritus by moving water. *Spec. Publ. SEPM*.

Hoffmann, T. (2015). Sediment residence time and connectivity in non-equilibrium and transient geomorphic systems. *Earth-Science Rev.* 150, 609–627. doi:10.1016/j.earscirev.2015.07.008.

Houssais, M., and Lajeunesse, E. (2012). Bedload transport of a bimodal sediment bed. *J. Geophys. Res. F Earth Surf.* 117, 1–13. doi:10.1029/2012JF002490.

Howard, A. D. (1994). A detachment-limited model of drainage basin evolution. *Water Resour. Res.* 30, 2261–2285. doi:10.1029/94WR00757.

Howard, A. D. A. D. (1982). Equilibrium and time scales in geomorphology: Application to sand-bed alluvial streams. *Earth Surf. Process. Landforms* 7, 303–325.

Hülscher, J., Fischer, G., Grunert, P., Auer, G., and Bernhardt, A. (2019). Selective recording of tectonic forcings in an Oligocene/Miocene submarine channel system: insights from new age constraints and sediment volumes from the Austrian Northern Alpine Foreland Basin. *Front. Earth Sci.* 7.

Hurst, M. D., Mudd, S. M., Walcott, R., Attal, M., and Yoo, K. (2012). Using hilltop curvature to derive the spatial distribution of erosion rates. *J. Geophys. Res. Earth Surf.* 117, 1–19. doi:10.1029/2011JF002057.

Jerolmack, D. J., and Mohrig, D. (2007). Conditions for branching in depositional rivers. *Geology*, 463–466. doi:10.1130/G23308A.1.

Jerolmack, D. J., and Paola, C. (2010). Shredding of environmental signals by sediment transport. *Geophys. Res. Lett.* 37, 1–5. doi:10.1029/2010GL044638.

Jobe, Z. R., Howes, N., Straub, K. M., Cai, D., Deng, H., Laugier, F., et al. (2020). Comparing aggradation, superelevation, and avulsion frequency of submarine and fluvial channels. *Front. Earth Sci.*

Jobe, Z. R., Sylvester, Z., Parker, A. O., Howes, N., Slowey, N., and Pirmez, C. (2015). Rapid Adjustment of Submarine Channel Architecture To Changes In Sediment Supply. *J. Sediment. Res.* 85, 729–753.

Jolivet, M., Barrier, L., Dominguez, S., Guerit, L., Heilbronn, G., and Fu, B. (2014). Unbalanced sediment budgets in the catchment–alluvial fan system of the Kuitun River (northern Tian Shan, China): Implications for mass-balance estimates, denudation and sedimentation rates in orogenic systems. *Geomorphology* 214, 168–182.

Jonell, T. N., Clift, P. D., Hoang, L. V., Hoang, T., Carter, A., Wittmann, H., et al. (2017). Controls on erosion patterns and sediment transport in a monsoonal, tectonically quiescent drainage, Song Gianh, central Vietnam. *Basin Res.* 29, 659–683. doi:10.1111/bre.12199.

Jonell, T. N., Li, Y., Blusztajn, J., Giosan, L., and Clift, P. D. (2018). Signal or noise? Isolating grain size effects on Nd and Sr isotope variability in Indus delta sediment provenance. *Chem. Geol.* 485, 56–73.

Kalińska, E., and Nartišs, M. (2014). Pleistocene and Holocene aeolian sediments of different location and geological history: A new insight from rounding and frosting of quartz grains. *Quat. Int.* 328–329, 311–322. doi:https://doi.org/10.1016/j.quaint.2013.08.038.

Kasprak, A., Wheaton, J. M., Ashmore, P. E., Hensleigh, J. W., and Peirce, S. (2015). The relationship between particle travel distance and channel morphology: Results from physical models of braided rivers. *J. Geophys. Res. Earth Surf.* 120, 55–74.

Kelly, R. F., Higuera, P. E., Barrett, C. M., and Sheng, F. (2011). A signal-to-noise index to quantify the potential for peak detection in sediment – charcoal records. *Quat. Res.* 75, 11–17. doi:10.1016/j.yqres.2010.07.011.

Kemp, D. B. (2012). Stochastic and deterministic controls on stratigraphic completeness and fidelity. *Int. J. Earth Sci.* 101, 2225–2238.

Kemp, D. B., and Sexton, P. F. (2014). Time-scale uncertainty of abrupt events in the geologic record arising from unsteady sedimentation. *Geology* 42, 891–894.

Kirchner, J. W., Dietrich, W. E., Iseya, F., and Ikeda, H. (1990). The variability of critical shear stress, friction angle, and grain protrusion in water-worked sediments. *Sedimentology* 37, 647–672. doi:10.1111/j.1365-3091.1990.tb00627.x.

Kooi, H., and Beaumont, C. (1994). Escarpment evolution on high-elevation rifted margins: Insights derived from a surface processes model that combines diffusion, advection, and reaction. *J.*

*Geophys. Res. Solid Earth* 99, 12191–12209.

Kooi, H., and Beaumont, C. (1996). Large-scale geomorphology: Classical concepts reconciled and integrated with contemporary ideas via a surface processes model. *J. Geophys. Res. Solid Earth* 101, 3361–3386.

Kothyari, U. C., and Jain, R. K. (2008). Influence of cohesion on the incipient motion condition of sediment mixtures. 44, 1–15. doi:10.1029/2007WR006326.

Kuenen, P. H. (1956). Experimental Abrasion of Pebbles: 2 . Rolling by Current. *J. Geol.* 64, 336–368.

Kujau, A., Nürnberg, D., Zielhofer, C., Bahr, A., and Röhl, U. (2010). Mississippi River discharge over the last ~560,000years — Indications from X-ray fluorescence core-scanning. *Palaeogeogr. Palaeoclimatol. Palaeoecol.* 298, 311–318. doi:https://doi.org/10.1016/j.palaeo.2010.10.005.

Lague, D., Crave, A., and Davy, P. (2003). Laboratory experiments simulating the geomorphic response to tectonic uplift. *J. Geophys. Res. Solid Earth* 108, ETG 3-1-ETG 3-20. doi:10.1029/2002jb001785.

Lamarre, H., MacVicar, B., and Roy, A. G. (2005). Using passive integrated transponder (PIT) tags to investigate sediment transport in gravel-bed rivers. *J. Sediment. Res.* 75, 736–741.

Lamb, M. P., Dietrich, W. E., and Venditti, J. G. (2008). Is the critical Shields stress for incipient sediment motion dependent on channel-bed slope ? 113, 1–20. doi:10.1029/2007JF000831.

Lenard, S. J. P., Lavé, J., France-lanord, C., Aumaître, G., Bourlès, D. L., and Keddadouche, K. (2020). Steady erosion rates in the Himalayas through late Cenozoic climatic changes. *Nat. Geosci.* doi:10.1038/s41561-020-0585-2.

Lewin, J., and Brewer, P. A. (2002). Laboratory simulation of clast abrasion. *Earth Surf. Process. Landforms J. Br. Geomorphol. Res. Gr.* 27, 145–164.

Li, C., Yang, S., Zhao, J., Dosseto, A., Bi, L., and Clark, T. R. (2016). The time scale of river sediment source-to-sink processes in East Asia. *Chem. Geol.* 446, 138–146.

Li, Q., Gasparini, N. M., and Straub, K. M. (2018a). Some signals are not the same as they appear: How do erosional landscapes transform tectonic history into sediment flux records? *Geology* 46, 407–410. doi:10.1130/G40026.1.

Li, Y., Clift, P. D., Böning, P., Blusztajn, J., Murray, R. W., Ireland, T., et al. (2018b). Continuous Holocene input of river sediment to the Indus Submarine Canyon. *Mar. Geol.* 406, 159–176.

Li, Y., Clift, P. D., and O'Sullivan, P. (2019). Millennial and centennial variations in zircon U-Pb ages in the quaternary indus submarine canyon. *Basin Res.* 31, 155–170.

Limaye, A. B. S., and Lamb, M. P. (2016). Numerical model predictions of autogenic fluvial terraces and comparison to climate change expectations. *J. Geophys. Res. Earth Surf.* 121, 512–544. doi:10.1002/2014JF003392.

Lupker, M., Lavé, J., France-lanord, C., Christl, M., Bourlès, D., Carcaillet, J., et al. (2017). 10Be systematics in the Tsangpo-Brahmaputra catchment: the cosmogenic nuclide legacy of the eastern Himalayan syntaxis. *Earth Surf. Dyn.* 5, 429–449. doi:10.5194/esurf-5-429-2017.

Mackin, J. H. (1948). Concept of the graded river. *Bull. Geol. Soc. Am.* 59, 463–512. Available at: papers2://publication/uuid/AC8A6716-22CC-43A5-80AE-59DCB5310A33.

Maier, K. L., Rosenberger, K. J., Paull, C. K., Gwiazda, R., Gales, J., Lorenson, T., et al. (2019). Sediment and organic carbon transport and deposition driven by internal tides along Monterey Canyon, offshore California. *Deep Sea Res. Part I Oceanogr. Res. Pap.* 153, 103108.

Malatesta, L., Avouac, J.-P., Brown, N. D., Breitenbach, S. F. M., Pan, J., Chevalier, M.-L., et al. (2018). Lag and mixing during sediment transfer across the Tian Shan piedmont caused by climate- driven aggradation-incision cycles. *Basin Res.* 30, 613–635. doi:10.1111/bre.12267.

Malatesta, L. C., Prancevic, J. P., and Avouac, J. P. (2017). Autogenic entrenchment patterns and terraces due to coupling with lateral erosion in incising alluvial channels. *J. Geophys. Res. Earth Surf.* 122, 335–355. doi:10.1002/2015JF003797.

Malmon, D. V, Dunne, T., and Reneau, S. L. (2003). Stochastic theory of particle trajectories through alluvial valley floors. *J. Geol.* 111, 525–542.

Malmon, D. V, Reneau, S. L., Dunne, T., Katzman, D., and Drakos, P. G. (2005). Influence of sediment storage on downstream delivery of contaminated sediment. *Water Resour. Res.* 41.

Mandal, S. K., Lupker, M., Burg, J.-P., Valla, P. G., Haghipour, N., Christl, M., et al. (2015). Spatial variability of 10Be-derived erosion rates across the southern Peninsular Indian escarpment: A key to landscape evolution across passive margins. *Earth Planet. Sci. Lett.* 425, 154–167. doi:10.1016/j.epsl.2015.05.050.

Mariotti, A., Blard, P.-H., Charreau, J., Petit, C., Molliex, S., and the ASTER Team (2019). Denudation systematics inferred from in situ cosmogenic 10Be concentrations in fine (50–100µm) and medium (100–250µm) sediments of the Var River basin, southern French Alps. *Earth Surf. Dyn.* 7, 1059–1074. doi:10.5194/esurf-7-1059-2019.

Mason, C. C., Fildani, A., Gerber, T., Blum, M. D., Clark, J. D., and Dykstra, M. (2017). Climatic and anthropogenic influences on sediment mixing in the Mississippi source-to-sink system using detrital zircons: Late Pleistocene to recent. *Earth Planet. Sci. Lett.* 466, 70–79. doi:10.1016/j.epsl.2017.03.001.

Mason, C. C., and Romans, B. W. (2018). Climate-driven unsteady denudation and sediment flux in a high-relief unglaciated catchment–fan using 26Al and 10Be: Panamint Valley, California. *Earth Planet. Sci. Lett.* 492, 130–143. doi:10.1016/j.epsl.2018.03.056.

Masteller, C. C., Finnegan, N. J., Turowski, J. M., Yager, E. M., and Rickenmann, D. (2019). History-Dependent Threshold for Motion Revealed by Continuous Bedload Transport Measurements in a Steep Mountain Stream. *Geophys. Res. Lett.* 46, 2583–2591. doi:10.1029/2018GL081325.

McCave, I. N., and Andrews, J. T. (2019). Distinguishing current effects in sediments delivered to the ocean by ice. I. Principles, methods and examples. *Quat. Sci. Rev.* 212, 92–107.

McCave, I. N., and Hall, I. R. (2006). Size sorting in marine muds: Processes, pitfalls, and prospects for paleoflow-speed proxies. *Geochemistry, Geophys. Geosystems* 7.

McInerney, F. A., and Wing, S. L. (2011). The Paleocene-Eocene Thermal Maximum: a perturbation of carbon cycle, climate, and biosphere with implications for the future. *Annu. Rev. Earth Planet. Sci.* 39, 489–516.

Métivier, F., and Gaudemer, Y. (1999). Stability of output fluxes of large rivers in South and East Asia during the last 2 million years: implications on floodplain processes. *Basin Res.* 11, 293–303. doi:10.1046/j.1365-2117.1999.00101.x.

Meyer-Peter, E., and Müller, R. (1948). Formulas for Bed-Load Transport. *IAHR*.

Miall, A. D. (2015). Updating uniformitarianism: stratigraphy as just a set of ‘frozen accidents.’ *Geol. Soc. London, Spec. Publ.* 404, 11–36.

Miller, A. J., and Kuehl, S. A. (2010). Shelf sedimentation on a tectonically active margin: a modern sediment budget for Poverty continental shelf, New Zealand. *Mar. Geol.* 270, 175–187.

Montgomery, D. R. (2001). Slope Distributions, Threshold Hillslopes, And Steady-State Topography. *Am. J. Sci.* 301, 432–454.

Moussirou, B., and Bonnet, S. (2018). Modulation of the erosion rate of an uplifting landscape by long-term climate change: An experimental investigation. *Geomorphology* 303, 456–466.

Mudd, S. M. (2017). Detection of transience in eroding landscapes. *Earth Surf. Process. Landforms* 42, 24–41. doi:10.1002/esp.3923.

Mulder, T., Migeon, S., Savoye, B., and Faugères, J.-C. (2001). Inversely graded turbidite sequences in the deep Mediterranean: a record of deposits from flood-generated turbidity currents? *Geo-Marine Lett.* 21, 86–93.

Muto, T., and Steel, R. J. (2001). Autostepping during the transgressive growth of deltas: results from flume experiments. *Geology* 29, 771–774.

Najafi, S., Dragovich, D., Heckmann, T., and Sadeghi, S. H. (2021). Sediment connectivity concepts and approaches. *Catena* 196, 104880. doi:10.1016/j.catena.2020.104880.

Nakamura, F., and Kikuchi, S. (1996). Some methodological developments in the analysis of sediment transport processes using age distribution of floodplain deposits. *Geomorphology* 16, 139–145.

Nesbitt, Hw., and Young, G. M. (1982). Early Proterozoic climates and plate motions inferred from major element chemistry of lutites. *Nature* 299, 715–717.

Nie, J., Ruetenik, G., Gallagher, K., Hoke, G., Garzione, C. N., Wang, W., et al. (2018). Rapid incision of the Mekong River in the middle Miocene linked to monsoonal precipitation. *Nat. Geosci.* 11, 944–948.

Normark, W. R., Hess, G. R., Stow, D. A. V, and Bowen, A. J. (1980). Sediment waves on the Monterey Fan levee: a preliminary physical interpretation. *Mar. Geol.* 37, 1–18.

O'Sullivan, G. J., Chew, D. M., Morton, A. C., Mark, C., and Henrichs, I. A. (2018). An integrated apatite geochronology and geochemistry tool for sedimentary provenance analysis. *Geochemistry, Geophys. Geosystems* 19, 1309–1326.

Ogston, A. S., Cacchione, D. A., Sternberg, R. W., and Kineke, G. C. (2000). Observations of storm and river flood-driven sediment transport on the northern California continental shelf. *Cont. Shelf Res.* 20, 2141–2162.

Olen, S. M., Bookhagen, B., Hoffmann, B., Sachse, D., Adhikari, D. P., and Strecker, M. R. (2015). Understanding erosion rates in the Himalayan orogen: A case study from the Arun Valley. *J. Geophys. Res. Earth Surf.* 120, 2080–2102. doi:10.1002/2014JF003410.Received.

Paola, C. (2016). A mind of their own: recent advances in autogenic dynamics in rivers and deltas. *SEPM Spec. Publ.* 106, 5–17.

Paola, C., and Foufoula-Georgiou, E. (2001). Statistical geometry and dynamics of braided rivers. *Gravel-Bed Rivers*, 47–71.

Paola, C., Heller, P., and Angevine, C. (1992). The large-scale dynamics of grain-size variation in alluvial basins, 1: Theory. *Basin Res.* 4, 73–90.

Parker, G., Klingeman, P. C., and McLean, D. G. (1982). Bedload and size distribution in paved gravel-bed streams. *J. Hydraul. Div.* 108, 544–571.

Parker, G., Toro-Escobar, C. M., Ramey, M., and Beck, S. (2003). Effect of floodwater extraction on mountain stream morphology. *J. Hydraul. Eng.* 129, 885–895.

Parsons, A. J., Michael, N. A., Whittaker, A. C., Duller, R. A., and Allen, P. A. (2012). Grain-size trends reveal the late orogenic tectonic and erosional history of the south– central Pyrenees, Spain. *J. Geol. Soc.* 169, 111–114. doi:10.1144/0016-76492011-087.SPECIAL.

Passchier, S., Ciarletta, D. J., Henao, V., and Sekkas, V. (2019). Sedimentary processes and facies on a high-latitude passive continental margin, Wilkes Land, East Antarctica. *Geol. Soc. London, Spec. Publ.* 475, 181–201.

Paull, C. K., Talling, P. J., Maier, K. L., Parsons, D., Xu, J., Caress, D. W., et al. (2018). Powerful turbidity currents driven by dense basal layers. *Nat. Commun.* 9, 1–9.

Pfeiffer, A. M., and Finnegan, N. J. (2018). Regional variation in gravel riverbed mobility, controlled by hydrologic regime and sediment supply. *Geophys. Res. Lett.* 45, 3097–3106.

Phillips, J. D., Marden, M., and Gomez, B. (2007). Residence time of alluvium in an aggrading fluvial system. *Earth Surf. Process. Landforms* 32, 307–316.

Piper, D. J. W. (1970). Transport and deposition of Holocene sediment on La Jolla deep sea fan, California. *Mar. Geol.* 8, 211–227.

Piper, D. J. W., and Normark, W. R. (1983). Turbidite depositional patterns and flow characteristics, Navy submarine fan, California Borderland. *Sedimentology* 30, 681–694.

Piper, D. J. W., and Normark, W. R. (2001). Sandy fans-from Amazon to Hueneme and beyond. *Am. Assoc. Pet. Geol. Bull.* 85, 1407–1438.

Ponton, C., West, A. J., Feakins, S. J., and Galy, V. (2014). Leaf wax biomarkers in transit record river catchment composition. *Geophys. Res. Lett.* 41, 6420–6427. doi:10.1002/2014GL061328.

Posamentier, H. W., and Kolla, V. (2003). Seismic geomorphology and stratigraphy of depositional elements in deep-water settings. *J. Sediment. Res.* 73, 367–388.

Prancevic, J. P., and Lamb, M. P. (2015). Unraveling bed slope from relative roughness in initial sediment motion. *J. Geophys. Res. Earth Surf.* 120, 474–489.

Prélat, A., and Hodgson, D. M. (2013). The full range of turbidite bed thickness patterns in submarine lobes: controls and implications. *J. Geol. Soc. London.* 170, 209–214.

Puchol, N., Charreau, J., Blard, P.-H., Lavé, J., Dominguez, S., Pik, R., et al. (2017). Limited impact of Quaternary glaciations on denudation rates in Central Asia. *GSA Bull.* 129, 479–499. doi:10.1130/B31475.1.

Puchol, N., Lavé, J., Lupker, M., Blard, P., Gallo, F., France-Lanord, C., et al. (2014). Grain-size dependent concentration of cosmogenic 10Be and erosion dynamics in a landslide-dominated Himalayan watershed. *Geomorphology* 224, 55–68. doi:10.1016/j.geomorph.2014.06.019.

Pudsey, C. J. (1992). Late Quaternary changes in Antarctic Bottom Water velocity inferred from sediment grain size in the northern Weddell Sea. *Mar. Geol.* 107, 9–33. doi:10.1016/0025-3227(92)90066-Q.

Quick, L., Sinclair, H. D., Attal, M., and Singh, V. (2019). Conglomerate recycling in the Himalayan foreland basin: Implications for grain size and provenance. *GSA Bull.*, 1–18. doi:10.1130/b35334.1.

Ramisch, A., Tjallingii, R., Hartmann, K., Diekmann, B., and Brauer, A. (2018). Echo of the Younger Dryas in Holocene lake sediments on the Tibetan Plateau. *Geophys. Res. Lett.*

Recking, A., Frey, P., Paquier, A., and Belleudy, P. (2009). An experimental investigation of mechanisms involved in bed load sheet production and migration. *J. Geophys. Res. Solid Earth* 114, 1–13. doi:10.1029/2008JF000990.

Repasch, M., Wittmann, H., Scheingross, J. S., Sachse, D., Szupiany, R., Orfeo, O., et al. (2020). Sediment transit time and floodplain storage dynamics in alluvial rivers revealed by meteoric 10Be. *J. Geophys. Res. Earth Surf.* 125, e2019JF005419.

Rohais, S., Bonnet, S., and Eschard, R. (2012). Sedimentary record of tectonic and climatic erosional perturbations in an experimental coupled catchment-fan system. *Basin Res.* 24, 198–212. doi:10.1111/j.1365-2117.2011.00520.x.

Romans, B. W., Castelltort, S., Covault, J. A., Fildani, A., and Walsh, J. P. (2016). Environmental signal propagation in sedimentary systems across timescales. *Earth-Science Rev.* 153, 7–29. doi:10.1016/j.earscirev.2015.07.012.

Romans, B. W., Normark, W. R., McGann, M. M., Covault, J. A., and Graham, S. A. (2009). Coarse-grained sediment delivery and distribution in the Holocene Santa Monica Basin, California: implications for evaluating source-to-sink flux at millennial time scales. *Geol. Soc. Am. Bull.* 121, 1394–1408.

Sachse, D., Billault, I., Bowen, G. J., Chikaraishi, Y., Dawson, T. E., Feakins, S. J., et al. (2012). Molecular Paleohydrology: Interpreting the Hydrogen-Isotopic Composition of Lipid Biomarkers from Photosynthesizing Organisms. *Annu. Rev. Earth Planet. Sci.* 40, 221–249. doi:10.1146/annurev-earth-042711-105535.

Sadler, P. M. (1981). Sediment Accumulation Rates and the Completeness of Stratigraphic Sections. *J. Geol.* 89, 569–584.

Sadler, P. M., and Jerolmack, D. J. (2015). Scaling laws for aggradation, denudation and progradation rates: the case for time-scale invariance at sediment sources and sinks. *Geol. Soc. London, Spec. Publ.* 404, 69–88. doi:10.1144/sp404.7.

Salles, T., Ding, X., and Brocard, G. (2018). pyBadlands: A framework to simulate sediment transport, landscape dynamics and basin stratigraphic evolution through space and time. *PLoS One* 13, e0195557.

Savi, S., Tofelde, S., Wickert, A., Bufe, A., Schildgen, T., and Strecker, M. (2020). Interactions between channels and tributary alluvial fans: channel adjustments and sediment-signal propagation. *Earth Surf. Dyn. Discuss.*, 1–46. doi:10.5194/esurf-2019-73.

Schaller, M., Blanckenburg, F. von, Hovius, N., Veldkamp, A., van den Berg, M. W., and Kubik, P. W. (2004). Paleoerosion Rates from Cosmogenic 10 Be in a 1.3 Ma Terrace Sequence: Response of the River Meuse to Changes in Climate and Rock Uplift . *J. Geol.* 112, 127–144. doi:10.1086/381654.

Schefuß, E., Eglinton, T. I., Spencer-Jones, C. L., Rullkötter, J., De Pol-Holz, R., Talbot, H. M., et al. (2016). Hydrologic control of carbon cycling and aged carbon discharge in the Congo River basin. *Nat. Geosci.* 9, 687–690.

Scheingross, J. S., Limaye, A. B., McCoy, S. W., and Whittaker, A. C. (2020). The shaping of erosional landscapes by internal dynamics. *Nat. Rev. Earth Environ.*, 1–16. doi:10.1038/s43017-020-0096-0.

Scheingross, J. S., Winchell, E. W., Lamb, M. P., and Dietrich, W. E. (2013). Influence of bed patchiness, slope, grain hiding, and form drag on gravel mobilization in very steep streams. *J. Geophys. Res. Earth Surf.* 118, 982–1001. doi:10.1002/jgrf.20067.

Schildgen, T. F., Robinson, R. A. J. J., Savi, S., Phillips, W. M., Spencer, J. Q. G. G., Bookhagen, B., et al. (2016). Landscape response to late Pleistocene climate change in NW Argentina: Sediment flux modulated by basin geometry and connectivity. *J. Geophys. Res.* 121, 1–23. doi:10.1002/2015JF003607.Received.

Schlunegger, F., and Norton, K. P. (2015). Climate vs . tectonics: the competing roles of Late Oligocene warming and Alpine orogenesis in constructing alluvial megafan sequences in the

North Alpine foreland basin. *Basin Res.* 27, 230–245. doi:10.1111/bre.12070.

Schmid, M., Ehlers, T. A., Werner, C., Hickler, T., and Fuentes-Espoz, J.-P. (2018). Effect of changing vegetation and precipitation on denudation--Part 2: Predicted landscape response to transient climate and vegetation cover over millennial to million-year timescales. *Earth Surf. Dyn.* 6.

Schmitz, B., and Pujalte, V. (2003). Sea-level, humidity, and land-erosion records across the initial Eocene thermal maximum from a continental-marine transect in northern Spain. *Geology* 31, 689–692.

Schmitz, B., and Pujalte, V. (2007). Abrupt increase in seasonal extreme precipitation at the Paleocene-Eocene boundary. *Geology* 35, 215–218. doi:10.1130/G23261A.1.

Schumm, S. A. (1977). *The fluvial system*. Wiley New York.

Schwenk, T., Spieß, V., Hübscher, C., and Breitzke, M. (2003). Frequent channel avulsions within the active channel–levee system of the middle Bengal Fan—an exceptional channel–levee development derived from Parasound and Hydrosweep data. *Deep Sea Res. Part II Top. Stud. Oceanogr.* 50, 1023–1045.

Sharman, G. R., Hubbard, S. M., Covault, J. A., Hinsch, R., Linzer, H., and Graham, S. A. (2018). Sediment routing evolution in the North Alpine Foreland Basin, Austria: interplay of transverse and longitudinal sediment dispersal. *Basin Res.* 30, 426–447.

Sharman, G. R., Sylvester, Z., and Covault, J. A. (2019). Conversion of tectonic and climatic forcings into records of sediment supply and provenance. *Sci. Rep.*, 1–7. doi:10.1038/s41598-019-39754-6.

Sheets, B. A., Hickson, T. A., and Paola, C. (2002). Assembling the stratigraphic record: Depositional patterns and time-scales in an experimental alluvial basin. *Basin Res.* 14, 287–301. doi:10.1046/j.1365-2117.2002.00185.x.

Shen, Z., Törnqvist, T. E., Autin, W. J., Mateo, Z. R. P., Straub, K. M., and Mauz, B. (2012). Rapid and widespread response of the Lower Mississippi River to eustatic forcing during the last glacial-interglacial cycle. *GSA Bull.* 124, 690–704. doi:10.1130/B30449.1.

Shields, A. (1936). Anwendung der Aehnlichkeitsmechanik und der Turbulenzforschung auf die Geschiebebewegung. *PhD Thesis Tech. Univ. Berlin* 26.

Simpson, G., and Castelltort, S. (2012). Model shows that rivers transmit high-frequency climate cycles to the sedimentary record. *Geology* 40, 1131–1134. doi:10.1130/G33451.1.

Sinclair, H. D., Stuart, F. M., Mudd, S. M., McCann, L., and Tao, Z. (2019). Detrital cosmogenic 21Ne records decoupling of source-to-sink signals by sediment storage and recycling in Miocene to present rivers of the Great Plains, Nebraska, USA. *Geology* 47, 3–6. doi:10.1130 /G45391.1.

Slingerland, R., and Smith, N. D. (2004). River avulsions and their deposits. *Annu. Rev. Earth Planet. Sci.* 32, 257–285.

Sommerfield, C. K., and Nittrouer, C. A. (1999). Modern accumulation rates and a sediment budget for the Eel shelf: a flood-dominated depositional environment. *Mar. Geol.* 154, 227–241.

Spychala, Y. T., Hodgson, D. M., Prélat, A., Kane, I. A., Flint, S. S., and Mountney, N. P. (2017). Frontal and lateral submarine lobe fringes: comparing sedimentary facies, architecture and flow processes. *J. Sediment. Res.* 87, 75–96.

Stacey, M. W., and Bowen, A. J. (1988). The vertical structure of density and turbidity currents: theory and observations. *J. Geophys. Res. Ocean.* 93, 3528–3542.

Stanley, S., and De Deckker, P. (2002). A Holocene record of allochthonous, aeolian mineral grains in an Australian alpine lake; implications for the history of climate change in southeastern Australia. *J. Paleolimnol.* 27, 207–219.

Sternberg, H. (1875). Untersuchungen uber Langen-und Querprofil geschiebefuhrender Flusse. *Zeitshrift fur Bauwes.* 25, 483–506.

Stoner, J. S., Channell, J. E. T., and Hillaire-Marcel, C. (1995). Magnetic properties of deep-sea sediments off southwest Greenland: Evidence for major differences between the last two deglaciations. *Geology* 23, 241–244.

Straub, K. M., Duller, R. A., Foreman, B. Z., and Hajek, E. A. (2020). Buffered, incomplete, and shredded: The challenges of reading an imperfect stratigraphic record. *J. Geophys. Res.*, 93. doi:10.1029/2019JF005079.

Straub, K. M., and Mohrig, D. (2008). Quantifying the morphology and growth of levees in aggrading submarine channels. *J. Geophys. Res. Earth Surf.* 113.

Strauss, D., and Sadler, P. M. (1989). Stochastic models for the completeness of stratigraphic sections. *Math. Geol.* 21, 37–59.

Suresh, P. O., Dosseto, A., Hesse, P. P., and Handley, H. K. (2014). Very long hillslope transport timescales determined from uranium-series isotopes in river sediments from a large, tectonically stable catchment. *Geochim. Cosmochim. Acta* 142, 442–457.

Talling, P. J. (2014). On the triggers, resulting flow types and frequencies of subaqueous sediment density flows in different settings. *Mar. Geol.* 352, 155–182.

Tejedor, A., Singh, A., Zaliapin, I., Densmore, A. L., and Foufoula-Georgiou, E. (2017). Scale-dependent erosional patterns in steady-state and transient-state landscapes. *Sci. Adv.* 3, e1701683.

Tipper, J. C. (1983). Rates of sedimentation, and stratigraphical completeness. *Nature* 302, 696–698.

Toby, S. C., Duller, R. A., Angelis, S. De, and Straub, K. M. (2019). A stratigraphic framework for the preservation and shredding of environmental signals. *Geophys. Res. Lett.*, 0–3. doi:10.1029/2019GL082555.

Tofelde, S., Duesing, W., Schildgen, T. F., Wickert, A. D., Wittmann, H., Alonso, R. N., et al. (2018). Effects of deep-seated versus shallow hillslope processes on cosmogenic 10Be concentrations in fluvial sand and gravel. *Earth Surf. Process. Landforms* 43, 3086–3098.

Tofelde, S., Savi, S., Wickert, A. D., Bufe, A., and Schildgen, T. F. (2019). Alluvial channel response to environmental perturbations: Fill-terrace formation and sediment-signal disruption. *Earth Surf. Dyn.* 7, 609–631. doi:10.5194/esurf-2018-84.

Tofelde, S., Schildgen, T. F., Savi, S., Pingel, H., Wickert, A. D., Bookhagen, B., et al. (2017). 100 kyr fluvial cut-and-fill terrace cycles since the Middle Pleistocene in the southern Central Andes, NW Argentina. *Earth Planet. Sci. Lett.* 473, 141–153. doi:10.1016/j.epsl.2017.06.001.

Toonen, W. H. J. J., Foulds, S. A., Macklin, M. G., and Lewin, J. (2017). Events, episodes, and phases: Signal from noise in flood-sediment archives. *Geology* 45, 331–334. doi:10.1130/G38540.1.

Toucanne, S., Zaragosi, S., Bourillet, J.-F., Dennielou, B., Jorry, S. J., Jouet, G., et al. (2012). External controls on turbidite sedimentation on the glacially-influenced Armorican margin (Bay of Biscay, western European margin). *Mar. Geol.* 303, 137–153.

Trampush, S. M., and Hajek, E. A. (2017). Preserving proxy records in dynamic landscapes: Modeling and examples from the Paleocene-Eocene Thermal Maximum. *Geology* 45, 967–970. doi:10.1130/G39367.1.

Tucker, G. E., and Slingerland, R. (1997). Drainage basin responses to climate change. *Water Resour. Res.* 33, 2031–2047. doi:10.1029/97WR00409.

Turowski, J. M. (2020). Mass balance, grade, and adjustment timescales in bedrock channels. 103–122. doi:10.5194/esurf-2019-47.

Turowski, J. M., Badoux, A., and Rickenmann, D. (2011). Start and end of bedload transport in gravel-bed streams. *Geophys. Res. Lett.* 38.

Val, P., Hoke, G. D., Fosdick, J. C., and Wittmann, H. (2016). Reconciling tectonic shortening, sedimentation and spatial patterns of erosion from10Be paleo-erosion rates in the Argentine Precordillera. *Earth Planet. Sci. Lett.* 450, 173–185. doi:10.1016/j.epsl.2016.06.015.

Van De Wiel, M. J., and Coulthard, T. J. (2010). Self-organized criticality in river basins: Challenging sedimentary records of environmental change. *Geology* 38, 87–90. doi:10.1130/G30490.1.

van den Berg van Saparoea, A.-P. H., and Postma, G. (2008). Control of climate change on the yield of river systems. *Recent Adv. Model. Siliciclastic Shallow-Marine Stratigr. SEPM Spec. Publ.* 90, 15–33. doi:10.2110/pec.08.90.0015.

van Dongen, R., Scherler, D., Wittmann, H., Blanckenburg, F. Von, von Blanckenburg, F., Dongen, R. Van, et al. (2019). Cosmogenic 10Be in river sediment: where grain size matters and why. *Earth Surf. Dyn.* 7, 393–410. doi:10.5194/esurf-7-393-2019.

Van Rijn, L. C. (2007). Unified view of sediment transport by currents and waves. I: Initiation of motion, bed roughness, and bed-load transport. *J. Hydraul. Eng.* 133, 649–667.

Völker, D., Reichel, T., Wiedicke, M., and Heubeck, C. (2008). Turbidites deposited on Southern Central Chilean seamounts: evidence for energetic turbidity currents. *Mar. Geol.* 251, 15–31.

Walsh, J. P., and Nittrouer, C. A. (2003). Contrasting styles of off-shelf sediment accumulation in New

Guinea. *Mar. Geol.* 196, 105–125.

Wang, H., Saito, Y., Zhang, Y., Bi, N., Sun, X., and Yang, Z. (2011). Recent changes of sediment flux to the western Pacific Ocean from major rivers in East and Southeast Asia. *Earth-Science Rev.* 108, 80–100.

Watkins, S. E., Whittaker, A. C., Bell, R. E., Brooke, S. A. S., Ganti, V., Gawthorpe, R. L., et al. (2020). Straight from the source's mouth: Controls on field-constrained sediment export across the entire active Corinth Rift, central Greece. *Basin Res.*

Watkins, S. E., Whittaker, A. C., Bell, R. E., McNeill, L. C., Gawthorpe, R. L., Brooke, S. A. S., et al. (2019). Are landscapes buffered to high-frequency climate change? A comparison of sediment fluxes and depositional volumes in the Corinth Rift, central Greece, over the past 130 ky. *GSA Bull.* 131, 372–388.

Weislogel, A. L., Graham, S. A., Chang, E. Z., Wooden, J. L., Gehrels, G. E., and Yang, H. (2006). Detrital zircon provenance of the Late Triassic Songpan-Ganzi complex: Sedimentary record of collision of the North and South China blocks. *Geology* 34, 97–100.

Weltje, G. J., and Tjallingii, R. (2008). Calibration of XRF core scanners for quantitative geochemical logging of sediment cores: Theory and application. *Earth Planet. Sci. Lett.* 274, 423–438. doi:https://doi.org/10.1016/j.epsl.2008.07.054.

Wheatcroft, R. A., and Sommerfield, C. K. (2005). River sediment flux and shelf sediment accumulation rates on the Pacific Northwest margin. *Cont. Shelf Res.* 25, 311–332.

Whipple, K. X. (2001). Fluvial landscape response time: How plausible is steady-state denudation? *Am. J. Sci.* 301, 313–325. doi:10.2475/ajs.301.4-5.313.

Whipple, K. X., and Tucker, G. E. (1999). Dynamics of the stream-power river incision model: Implications for height limits of mountain ranges, landscape response timescales, and research needs. *J. Geophys. Res. Solid Earth* 104, 17661–17674. doi:10.1029/1999jb900120.

Whittaker, A. C., Attal, M., and Allen, P. A. (2010). Characterising the origin, nature and fate of sediment exported from catchments perturbed by active tectonics. *Basin Res.* 22, 809–828. doi:10.1111/j.1365-2117.2009.00447.x.

Whittaker, A. C., Attal, M., Cowie, P. A., Tucker, G. E., and Roberts, G. (2008). Decoding temporal and spatial patterns of fault uplift using transient river long profiles. 100, 506–526. doi:10.1016/j.geomorph.2008.01.018.

Whittaker, A. C., Duller, R. A., Springett, J., Smithells, R. A., Whitchurch, A. L., and Allen, P. A. (2011). Decoding downstream trends in stratigraphic grain size as a function of tectonic subsidence and sediment supply. *GSA Bull.* 123, 1363–1382. doi:10.1130/B30351.1.

Wiberg, P. L., and Smith, J. D. (1987). Calculations of the critical shear stress for motion of uniform and heterogeneous sediments. *Water Resour. Res.* 23, 1471–1480.

Wickert, A. D., and Schildgen, T. F. (2019). Long-profile evolution of transport-limited gravel-bed rivers. *Earth Surf. Dyn.* 7, 17–43.

Wilcock, P. R., and Crowe, J. C. (2003). Surface-based transport model for mixed-size sediment. *J. Hydraul. Eng.* 129, 120–128. doi:10.1061/(ASCE)0733-9429(2003)129.

Willenbring, J. K., Gasparini, N. M., Crosby, B. T., and Brocard, G. (2013). What does a mean mean? The temporal evolution of detrital cosmogenic denudation rates in a transient landscape. *Geology* 41, 1215–1218. doi:10.1130/G34746.1.

Willett, S. D., and Brandon, M. T. (2002). On steady states in mountain belt. *Geology* 30, 175–178. doi:10.1130/0091-7613(2002)030<0175:OSSIMB>2.0.CO;2.

Wittmann, H., Oelze, M., Gaillardet, J., Garzanti, E., and von Blanckenburg, F. (2020). A global rate of denudation from cosmogenic nuclides in the Earth's largest rivers. *Earth-Science Rev.*, 103147.

Wittmann, H., von Blanckenburg, F., Dannhaus, N., Bouchez, J., Gaillardet, J., Guyot, J.-L., et al. (2015). A test of the cosmogenic 10Be (meteoric)/9Be proxy for simultaneously determining basin-wide erosion rates, denudation rates, and the degree of weathering in the Amazon basin. *J. Geophys. Res. Earth Surf.* 120, 2498–2528.

Wittmann, H., von Blanckenburg, F., Maurice, L., Guyot, J. L., and Kubik, P. W. (2011). Recycling of Amazon floodplain sediment quantified by cosmogenic 26Al and 10Be. *Geology* 39, 467–470. doi:10.1130/G31829.1.

Yuan, X. P., Braun, J., Guerit, L., Rouby, D., and Cordonnier, G. (2019a). A New Efficient Method to Solve the Stream Power Law Model Taking Into Account Sediment Deposition. *J. Geophys. Res. Earth Surf.* doi:10.1029/2018JF004867.

Yuan, X. P., Braun, J., Guerit, L., Simon, B., Bovy, B., Rouby, D., et al. (2019b). Linking continental erosion to marine sediment transport and deposition: A new implicit and O(N) method for inverse analysis. *Earth Planet. Sci. Lett.* 524. doi:10.1016/j.epsl.2019.115728.

Zanke, U. C. E. (2003). On the influence of turbulence on the initiation of sediment motion. *Int. J. Sediment Res.* 18, 17–31.

Zapata, F., and Nguyen, M.-L. (2009). Soil erosion and sedimentation studies using environmental radionuclides. *Radioact. Environ.* 16, 295–322.

Zhang, J., Sylvester, Z., and Covault, J. (2020). How do basin margins record long-term tectonic and climatic changes ? XX, 1–5. doi:10.1130/G47498.1/5051425/g47498.pdf.

Zolitschka, B., Francus, P., Ojala, A. E. K., and Schimmelmann, A. (2015). Varves in lake sediments–a review. *Quat. Sci. Rev.* 117, 1–41.